Coupled Attitude And Orbital Control System Using Spacecraft Simulators

Scott Evan Lennox

Thesis submitted to the Faculty of the
Virginia Polytechnic Institute and State University
in partial fulfillment of the requirements for the degree of

Master of Science
in
Aerospace Engineering

Dr. Christopher D. Hall, Committee Chair
Dr. Hanspeter Schaub, Committee Member
Dr. Craig A. Woolsey, Committee Member

July 7, 2004
Blacksburg, Virginia

Keywords: Coupled Control, Attitude Control, Orbital Control, Spacecraft Simulators, Air Bearings

Coupled Attitude And Orbital Control System Using Spacecraft Simulators

Scott Evan Lennox

(ABSTRACT)

Translational and rotational motion are coupled for spacecraft performing formation flying missions. This motion is coupled because orbital control is dependent on the spacecraft attitude for vectored thrust. Formation flying spacecraft have a limited mass and volume for propulsion systems. We want to maximize the efficiency of the spacecraft, which leads to minimizing the error introduced by thrusting in the wrong direction. This thrust direction error leads to the need for a coupled attitude and orbital control strategy. In this thesis a coupled control system is developed using a nonlinear Lyapunov attitude controller and a nonlinear Lyapunov-based orbital controller. A nonlinear Lyapunov attitude controller is presented for a spacecraft with three-axis momentum wheel control. The nonlinear Lyapunov-based orbital controller is combined with a mean motion control strategy to provide a globally asymptotically stable controller. The attitude and orbit control laws are verified separately using numerical simulation, and then are integrated into a coupled control strategy. The coupled system simulations verify that the coupled control strategy is able to correct for an initial relative position error between two spacecraft.

Dedication

In memory of Dr. Frederick H. Lutze, Jr. for always having an open door to talk about work, life and particularly Virginia Tech sports. I will never forget those five minute questions that would turn into hour long conversations about everything and nothing, I only regret that we weren't able to have more of them. (November 27, 1937 – December 2, 2003)

Acknowledgments

This work could not have been completed without the help and support from numerous individuals. I would like to acknowledge Dr. Christopher Hall for being my advisor for four years. Dr. Hall mentored me through all of my aerospace engineering projects, specifically, my tenure as the Systems Lead for HokieSat and my Master's Degree research. I would like to thank Dr. Hanspeter Schaub and Dr. Craig Woolsey for being members of my committee. Thank you both for being around when I needed advice throughout my research.

I also would like to thank the Aerospace and Ocean Engineering Department staff that have been very helpful and always available when I needed them.

I would like to thank the current and past members of the Space System Simulation Laboratory. Everyone has helped me with my research and my enjoyment of graduate school. A special thank you to Jana Schwartz and Matthew VanDyke for helping derive and debug my research. This research would not be complete if it was not for your help.

I would also like to thank all of my friends that I have made at Virginia Tech and my friends from Charlottesville that have not disowned me these past six years.

Lastly, I would like to thank my family: Mom, Dad, Aaron, Becky, Sarah, Emily, and Jacob. I wouldn't be anywhere with out all of your love and support.

"It's not the size of the diploma that matters,
it's the quality of the degree."
– Dr. Roger Avery, Senior Associate Dean

Contents

List of Figures

List of Tables

Nomenclature

a	Semi-major axis
a^{**}	Target semi-major axis calculated using the mean motion control strategy
α	Constant for the analytic solution of the Hill-Clohessy-Wiltshire equations of motion
$\mathbf{a}_p$	Accelerations due to perturbations
A	Matrix containing the axial unit vectors of the momentum wheels ($3 \times N$)
$A_\circ$	Constant for the analytic solution of the Hill-Clohessy-Wiltshire equations of motion
b	Semi-minor axis
d	The distance between the ideal position and the attitude error position
e	Eccentricity
$\hat{\mathbf{e}}$	Euler axis
$E_\circ$	Initial eccentric anomaly
E_t	Eccentric anomaly after Δt
ΔE	Change in eccentric anomaly ($E_t - E_\circ$)
$\mathcal{E}$	Total energy of an orbit
$\boldsymbol{\eta}$	Vector of differential changes in the first five orbital elements (a, e, i, ω, Ω)
f_E	f equation from the f and g method in terms of eccentric anomaly
g	Magnitude of the net applied torque about the mass center
g_E	g equation from the f and g method in terms of eccentric anomaly
$\mathbf{g}$	Net applied torque about the mass center
$\mathbf{g}_a$	Matrix of the internal torques applied by momentum wheels
$\mathbf{g}_e$	Matrix of the external torques applied to the spacecraft
$g_{\max}$	Maximum applied torque
$G(\boldsymbol{\sigma})$	Matrix relating the $\boldsymbol{\omega}$ and the $\dot{\boldsymbol{\sigma}}$
h	Magnitude of the angular momentum vector
h_o	Magnitude of the orbit momentum vector
$\mathbf{h}$	Angular momentum vector
$\mathbf{h}_a$	Matrix of the axial angular momenta of the wheels
$\mathbf{h}_B$	System angular momentum vector
$\mathbf{h}_o$	Orbit momentum vector
H	Input matrix for the equations of motion for the five orbital elements

$\tilde{H}$	Input matrix for the equations of motion for the orbital elements
i	Inclination
I	Moment of inertia matrix of the entire spacecraft
$I_{\max}$	Maximum moment of inertia
I_s	Axial moment of inertia matrix for N number of momentum wheels
I_3	Identity matrix
$\hat{I}$	Unit vector in the vernal equinox direction for the Earth-centered inertial reference frame
J	A positive definite inertia-like matrix $(I - AI_sA^{\mathsf{T}})$
$\hat{J}$	Unit vector to define the equatorial plane with $\hat{I}$ in the Earth-centered inertial reference frame
k_1	Attitude gain
k_2	Angular velocity gain
K	A positive-definite matrix equal to its transpose
$\hat{K}$	Unit vector in the direction of the Earth's spin axis for the Earth-centered inertial reference frame
$\tilde{K}$	Vector of the first five orbital control gains
K_a	Control gain on the semi-major axis
K_e	Control gain on the eccentricity
K_i	Control gain on the inclination
K_n	Control gain on the mean motion
K_ω	Control gain on the argument of periapse
K_Ω	Control gain on the right ascension of the ascending node
l	An integer
m	Mass of the spacecraft
μ	Gravitational parameter
M	Mean anomaly
M_t	Mean anomaly after Δt
$M_\circ$	Initial mean anomaly
n	Mean motion
ν	True anomaly
N	Number of momentum wheels
$\hat{\mathbf{o}}_r$	Unit vector in the radial direction for the Hill reference frame
$\hat{\mathbf{o}}_h$	Unit vector in orbit normal direction of the chief spacecraft for the Hill reference frame
$\hat{\mathbf{o}}_1$	Unit vector in the direction that completes the right-handed coordinate frame for the orbital reference frame
$\hat{\mathbf{o}}_2$	Unit vector in the negative orbit normal direction for the orbital reference frame
$\hat{\mathbf{o}}_3$	Unit vector in the nadir direction for the orbital reference frame
$\hat{\mathbf{o}}_\theta$	Unit vector in the direction that completes the right-handed coordinate frame for the Hill frame

$\mathbf{O}$	Center of the Earth
$\mathbf{œ}$	Vector of orbital elements $[a\ e\ i\ \Omega\ \omega\ M]^T$
ω	Argument of periapse
$\boldsymbol{\omega}$	Angular velocity
$\boldsymbol{\omega}_c$	Actual angular velocity of the spacecraft
$\boldsymbol{\omega}_d$	Desired angular velocity of the spacecraft
$\boldsymbol{\omega}_s$	Axial angular velocity matrix of the momentum wheels with respect to the body $(N \times 1)$
$\boldsymbol{\omega}_B$	Angular velocity matrix of the body frame expressed in the inertial frame (3×1)
Ω	Right ascension of the ascending node
$\boldsymbol{\delta\omega}$	Difference between the desired angular velocity and current angular velocity
p	Semi-latus rectum
ϕ	Rotation angle about major axis
$\phi_\circ$	Initial rotation angle about major axis
ψ	Attitude error
Φ	Euler angle
$\Delta\phi$	Change in rotation angle $(\phi - \phi_\circ)$
r	Magnitude of the position vector $\mathbf{r}$
$\mathbf{r}$	Position vector
$r_\circ$	Magnitude of the initial position vector
r_t	Magnitude of the position vector after Δt
$\mathbf{r}_{\text{int}}$	Initial in-track error
$\mathbf{r}_{t_\circ}$	Initial position vector of the "rendezvous" spacecraft
$\mathbf{r}_t$	Position vector after Δt
$\mathbf{r}_{t,0}$	Ideal position at time t
$\mathbf{r}_{t,\psi}$	Position at time t with attitude error ψ
$\mathbf{r}_\circ$	Initial position vector
R	Rotation matrix
R^{ad}	Rotation matrix due to attitude error
R^{cd}	Rotation matrix between the actual and desired attitude of the spacecraft
σ_*	Components of the MRP where $* = 1, 2$ and 3
$\boldsymbol{\sigma}$	Modified Rodrigues Parameters
$\boldsymbol{\sigma}^s$	Shadow set of Modified Rodrigues Parameters
$\boldsymbol{\delta\sigma}$	Rotational error between the desired attitude and the current attitude of the spacecraft
t	Time
$t_\circ$	Initial time
t_1	Time estimate for the nonlinear attitude controller to complete the attitude maneuver
t_2	Time after the thrust has been applied using the orbital estimator
t_{oc}	Thrust time used in the orbital controller

θ	Argument of latitude
$\mathbf{T}_{\text{ideal}}$	Ideal thrust vector
$\mathbf{t}_{t_\circ}$	Initial position of the target spacecraft
$\mathbf{t}_t$	Position of the target spacecraft at time t
T_{mag}	Magnitude of the thrust vector
$\mathbf{T}$	Thrust vector with an attitude error
$\hat{\mathbf{T}}$	Thrust direction in the Hill frame
$\tilde{\mathbf{T}}$	Thruster orientation in the body frame
Δt	Change in time $(t - t_\circ)$
Δt_t	Thruster fire duration
u_h	Orbit normal control acceleration
u_r	Radial control acceleration
u_θ	Transverse control acceleration
$\mathbf{u}$	Control acceleration vector $[u_r\ u_\theta\ u_h]^T$
$v_\circ$	Magnitude of the initial velocity
$\mathbf{v}$	Initial velocity vector of the "rendezvous" spacecraft
$\mathbf{v}_i$	Spacecraft velocity plus impulsive thrust
$\mathbf{v}_t$	Velocity vector after Δt
$\mathbf{v}_{t,\psi}$	Velocity at time t with attitude error
$\mathbf{v}_\circ$	Initial velocity vector
V	Candidate Lyapunov function
Δv	Change in velocity
x	Position in the radial direction for the Hill frame
$x_\circ$	Initial relative position in the radial direction
$\dot{x}_\circ$	Initial relative velocity in the radial direction
$\dot{x}_\circ^e$	Initial relative velocity in the radial direction with an attitude error
$\dot{x}_\circ^i$	Initial relative velocity in the radial direction for the ideal case
x_{off}	Integration constant
y	Position in the direction that completes the right-handed Hill frame
$y_\circ$	Initial relative position in the y direction of the Hill frame
$\dot{y}_\circ$	Initial relative velocity in the y direction of the Hill frame
$\dot{y}_\circ^e$	Initial relative velocity in the y direction of the Hill frame with an attitude error
$\dot{y}_\circ^i$	Initial relative velocity in the y direction of the Hill frame for the ideal case
y_{off}	Integration constant
z	Position in the $\hat{\mathbf{o}}_h$ direction for the Hill frame
$z_\circ$	Initial relative position in the orbit momentum direction
$(\cdot)^*$	Target orbital element
$(\cdot)^{\text{T}}$	The transpose of a matrix
$[(\cdot)\times]$	Skew symmetric matrix of $(\cdot)$
$\delta(\cdot)$	A differential change in $(\cdot)$
$\dot{(\cdot)}$	The first time derivative of $(\cdot)$

$\ddot{(\cdot)}$	The second time derivative of $(\cdot)$
$(\cdot) \times (\cdot)$	The cross product of two vectors
$(\cdot) \cdot (\cdot)$	The dot product of two vectors

Abbreviations

CAD	Computer Aided Design
DSACSS	Distributed Spacecraft Attitude Control System Simulator
GEC	Geospace Electrodynamic Connections
GEONS	GPS Enhanced Onboard Navigation System
GPS	Global Positioning System
ION-F	Ionospheric Observation Nanosatellite Formation
LISA	Laser Interferometer Space Antenna
MMS	Magnetospheric Multiscale
MRPs	Modified Rodrigues Parameters
ST3	Space Technology 3
ST5	Space Technology 5
ST9	Space Technology 9
SPECS	Submillimeter Probe of the Evolution of Cosmic Structure
TPF	Terrestrial Planet Finder

Chapter 1

Introduction

In the last few years the space industry has started to change its focus from single large satellite missions to the use of many smaller satellites flying in formations. The concept of small satellites flying in close proximity can increase the performance, reliability and versatility, and decrease the cost of the space missions.

The concept of spacecraft flying in close proximity was first discussed in the fictional work by Kurd Lassnitz in the late 19$^{\text{th}}$ century where he discussed the concept of a satellite rendezvousing with a satellite base in orbit about Earth.[1] Yuri Vasil'yevich Kondratyuk was the first person to publish literature about the concept of rendezvous as we know it today. Kondratyuk discussed the idea of matching the orbits of the two spacecraft and the need for instruments that would control the guidance of the spacecraft in 1916.[2] The first spacecraft rendezvous occurred in December of 1965 by Gemini VI, when Gemini VI and Gemini VII performed station keeping maneuvers to keep the separation distance between the two spacecraft between 0.3 meter and 90 meters. The first successful docking of two spacecraft was performed by Gemini VIII in March of 1966 and the first autonomous docking of two spacecraft occurred in October of 1967 by the Soviet spacecraft Cosmos 186 and Cosmos 188.[3] These early missions led to the development of many other missions that required spacecraft to fly in close proximity, including the first autonomous formation flying maneuver performed by NASA's Earth Observing-1 spacecraft and Landsat7.

Many of the current formation flying missions are focused on space interferometry such as the Submillimeter Probe of the Evolution of Cosmic Structure (SPECS) and the Terrestrial Planet Finder (TPF).[4,5] Some of the other current formation flying missions include Space Technology 5 (ST5), Space Technology 9 (ST9), and Aura.[6,7,8] These missions are just a few of the formation flying missions that are currently in various phases of development.

1.1 Motivation

Formation flying presents many interesting and difficult problems that have not been thoroughly researched. One of these topics is the idea of coupling the spacecraft's attitude and orbital control systems. Coupling the attitude and orbital control systems is required because the translational and rotational motion is coupled.

The coupled translational and rotational motion becomes more apparent in spacecraft with physical and operational constraints associated with the translational and rotational motion. Formation flying spacecraft have physical and operation constraints associated with thrust vectoring. An example of a physical constraint is the reduced volume and mass allotted for the orbital propulsion system. In many cases there may be one or two thrusters that need to be reoriented in the correct direction before an orbital maneuver can be executed. Many of these small spacecraft use low thrust propulsion systems that require almost continuous thrust. The thrust direction error needs to be minimized to maximize the efficiency of these spacecraft, which leads to a coupled orbital and attitude control system. The operations of a formation may also lead to a relative position constraint. This relative position constraint requires a low thrust propulsion system to be able to change the spacecraft's position with accuracy on the thrust direction. This accuracy is coupled with the attitude control system accuracy, thus the need for a coupling of the attitude and orbital control systems.

1.2 Problem Definition

The purpose of this research is to develop and implement a coupled attitude and orbital control system using an existing attitude control law and an existing orbital control law for the use in spacecraft formation flying missions. There are numerous control strategies that have been separately developed for attitude control and orbital control. The coupled system needs to be modular to allow for the testing of these separate control strategies in a coupled system. The coupled system needs to be developed for implementation using Virginia Tech's Distributed Spacecraft Attitude Control System Simulator (DSACSS).[9]

1.3 Approach

We simplify the formation flying problem to the rendezvous problem where the spacecraft knows its location (we call this location the "rendezvous" spacecraft), and its desired position (we call this position the "target" spacecraft). We consider the target spacecraft as a passive spacecraft and the rendezvous spacecraft as a controllable spacecraft. The target spacecraft is in an orbit that is known to the rendezvous spacecraft. We assume that the rendezvous spacecraft has one variable thrust thruster and a three-axis momentum wheel system for attitude control. We also assume an ideal space environment without disturbance forces.

We use an orbital controller to determine the ideal thrust direction to perform the orbital maneuver. The thruster needs to be aligned with this ideal thrust direction, which may require an attitude maneuver to occur. We choose a nonlinear attitude controller and a nonlinear orbital controller as the primary control laws for the coupled system. A linear bang-bang attitude controller is developed to estimate the time required for the nonlinear attitude controller to perform the required attitude maneuver. These controllers and an orbital propagator are used to develop the coupled system. We perform separate numerical simulations on both the nonlinear attitude controller and nonlinear orbital controller for validation of the control strategies. We also perform numerical simulations on the coupled system to validate the coupled system strategy.

1.4 Overview

In Chapter 2, we present a literature review that includes previous work on attitude control laws, orbital control laws, relative orbits for spacecraft formation flying, coupled attitude and orbital control strategies, and Virginia Tech's DSACSS System.

We present the attitude kinematics and the attitude and orbital equations of motion in Chapter 3. We assume three-axis attitude control using N momentum wheels. We present the attitude equations of motion in terms of Modified Rodrigues Parameters (MRPs) and the orbital equations of motion in terms of the classical orbital elements.

The linear bang-bang and the nonlinear Lyapunov attitude controllers are presented in Chapter 4. We also present the nonlinear Lyapunov-based feedback orbital controller with mean motion control strategy in Chapter 4.

In Chapter 5, we present the coupled attitude and orbital control system. We also present a two-body orbital propagator and a method for determining the maximum allowable attitude error between the desired attitude and the actual attitude for the thruster to fire.

Numerical simulations are performed in Chapter 6 on the nonlinear Lyapunov attitude controller and nonlinear Lyapunov-based feedback orbital controller with mean motion control strategy using Matlab©. These results are compared to the results found from the numerical simulations of the coupled system, which are also performed using Matlab©.

Chapter 7 presents a summary and the conclusions of the work presented in this thesis. We also present some recommendations for future work to be completed using the coupled attitude and orbital control system. We also discuss a basic overview of how to implement the coupled control system on Virginia Tech's Distributed Spacecraft Attitude Control System Simulator.

Chapter 2

Literature Review

In this chapter, we present a review of the attitude and orbital control strategies developed for formation flying. We introduce some the possible applications for the coupled attitude and orbital control system. We also discuss articles pertaining to attitude controllers, orbital controllers, and coupled attitude and orbital controllers. We conclude this chapter with a discussion of Virginia Tech's Distributed Spacecraft Attitude Control System Simulator (DSACSS).

2.1 Applications

The coupled attitude and orbital control system is designed for use in formation flying missions, but it is reasonable to assume that other single spacecraft missions can benefit from the use of the coupled attitude and orbital control system. The use of a coupled attitude and orbital control system is beneficial for all spacecraft missions because the translational and rotational motion is coupled. This coupling becomes more apparent in spacecraft that have constraints on the thrust direction. Small spacecraft are more likely to have thrust direction constraints than larger spacecraft. We will see an increase in the number of thrust direction constrained satellites with the increasing emphasis on small satellites flying in formation.

Some of the proposed formation flying missions that would benefit from a coupled system include: Aura, Geospace Electrodynamic Connections (GEC), Ionospheric Observation Nanosatellite Formation (ION-F), Laser Interferometer Space Antenna (LISA), Magnetospheric Multiscale (MMS), SPECS, ST5, ST9, TechSat-21, and TPF.[8,10,11,12,13,4,6,7,14,5]

2.2 Attitude Controllers

There are numerous control methods available to control the attitude of a spacecraft. The attitude control system of a spacecraft is dependent on the available spacecraft actuators for attitude control. Some of the common actuators used on spacecraft are control moment gyros, magnetic torquers, momentum wheels, reaction wheels, and thrusters.[15] In this section we describe some of the different attitude control strategies.

Many of the control methods used on current spacecraft are linear controllers, but spacecraft dynamics are nonlinear, thus a nonlinear controller could be a more effective solution to control a spacecraft's attitude motion. Tsiotras presented eight different nonlinear feedback control laws using Lyapunov functions with quadratic and logarithmic terms in Ref. 16. These control laws use Euler Parameters, Cayley-Rodrigues Parameters and Direction Cosines. These controllers were expanded to include Modified Rodrigues Parameters in Ref. 17. Hall *et al.* used a Modified Rodrigues Parameter Lyapunov function to derive three attitude tracking controllers using thrusters and momentum wheels.[17] The three controllers were proven to be globally asymptotically stable using LaSalle's Theorem. Tsiotras *et al.* expanded on these attitude tracking controllers to include energy storage using the momentum wheels for an integrated power and attitude-control system.[18] Schaub *et al.* used a nonlinear feedback control law to control a spacecraft's nonlinear dynamics realizing the linear closed-loop dynamics of the system.[19] An adaptive control law was developed to enforce the closed-loop dynamics with large errors in the moments of inertia and external disturbances. Xing and Parvez derived a nonlinear Lyapunov controller and a robust sliding controller for the tracking control problem.[20] They converted the tracking control problem into a regulator problem using the relative attitude state equations. Transforming the tracking problem into a regulator problem simplifies the design procedure of the controllers.[20]

2.3 Orbital Controllers

Controlling the orbit of a spacecraft is accomplished using a propulsion system. There are many different types of propulsion systems, but they all change the orbit of a spacecraft by applying a force to the spacecraft.[21] Similar to the attitude controllers, there are numerous control methods available to control the spacecraft's orbit. For most space missions, orbital maneuvering is controlled by the ground station, but formation flying leads to the use of autonomous orbital control for formation keeping.

Most of the orbital controllers that have been developed for formation flying missions have used the linearized equations of relative motion for two objects under the influence of a point-mass gravitational field. These equations are commonly known as the Hill-Clohessy-Wiltshire equations. Hill discussed these equations in Ref. 22 and Clohessy and Wiltshire discussed these equations in Ref. 23. The equations of motion expressed in the Hill reference frame are

$$\ddot{x} - 2n\dot{y} - 3n^2 x = F_x \tag{2.1}$$

$$\ddot{y} + 2n\dot{x} = F_y \tag{2.2}$$

$$\ddot{z} + n^2 z = F_z \tag{2.3}$$

where x, z, and y are the distances in the orbit radius direction, the orbit normal direction of the reference spacecraft, and the direction that completes the right-handed coordinate frame respectively, F_x, F_y, and F_z are the perturbation or control accelerations in the Hill frame, and n is the mean motion of the reference spacecraft. These equations are valid when the reference spacecraft is in a circular orbit and the distances between the spacecraft are small in comparison to the orbital radii. When the forces acting on the spacecraft are zero, the analytic solutions to Equations (2.1)–(2.3) are[23]

$$x(t) = \frac{\dot{x}_\circ}{n}\sin nt - \left(3x_\circ + \frac{2\dot{y}_\circ}{n}\right)\cos nt + 4x_\circ + \frac{2\dot{y}_\circ}{n} \tag{2.4}$$

$$y(t) = \frac{2\dot{x}_\circ}{n}\cos nt + \left(6x_\circ + \frac{4\dot{y}_\circ}{n}\right)\sin nt - \left(6nx_\circ + 3\dot{y}_\circ\right)t - \frac{2\dot{x}_\circ}{n} + y_\circ \tag{2.5}$$

$$z(t) = \frac{\dot{z}_\circ}{n}\sin nt + z_\circ \cos nt \tag{2.6}$$

where t is the time, and $x_\circ$, $y_\circ$, $z_\circ$, $\dot{x}_\circ$, $\dot{y}_\circ$, and $\dot{z}_\circ$ are the initial conditions on the relative position and velocity.

A controller that uses the Hill-Clohessy-Wiltshire equations was presented in Ref. 24. Kapila *et al.* presented a linear controller for formation keeping of a leader-follower spacecraft formation. The simulations presented in this article did not include any orbital perturbations. Sabol *et al.* examined four different spacecraft formations using the Hill-Clohessy-Wiltshire equations and determined that the orbital perturbations have a significant effect on the ability of the spacecraft to maintain the formation.[25] The perturbations affected each formation uniquely which suggests that perturbations need to be included in formation-keeping controllers. A linear controller that was derived from the Hill-Clohessy-Wiltshire equations with perturbations was presented in Ref. 26. The relative position error was set to be ±21 meters. This relative position error is large in comparison to some of the current mission requirements. We can use a nonlinear controller that could reduce the relative position error because the nonlinear controller can account for the nonlinear orbital dynamics. Vaddi and Vadali presented a linear quadratic regulator, nonlinear Lyapunov, and period matching controllers.[27] These controllers are valid for both circular and elliptical reference orbits. The relative position errors were not reported in this reference.

Another way to describe the relative motion of formation flying spacecraft is to use differential orbital elements. Schaub and Alfriend presented a hybrid continuous feedback control law for a local Cartesian relative orbit frame and as a function of differential orbital elements.[28] These control laws are valid for both circular and elliptical orbits. Schaub and Alfriend also present a direct mapping between the local Cartesian position and velocity to the differential orbital elements. Schaub *et al.* presented two nonlinear feedback control laws using mean orbital element differences in Ref. 29. The use of mean elements allows for the specification of the relative orbit geometry using the mean of the orbital elements (mean elements) and the instantaneous, time varying components (osculating elements) as the errors in the relative orbit geometry.[29] Ilgen developed a Lyapunov-optimal feedback control law for orbital maneuvers.[30] This control law uses Gauss' form of Lagrange's planetary equations in classical and equinoctial orbital-element forms. Naasz and Hall[31] developed a nonlinear Lyapunov-based control law with mean-motion control to perform autonomous orbital maneuvers for formation flying. This control law can be used for formation-keeping and formation-maneuvering.

2.4 Coupled Controllers

The coupling of the attitude and orbital control systems is a relatively new concept and there are only a few published papers. Wang and Hadaegh derived and implemented attitude and orbital control laws in a simulation of microspacecraft flying in formations in Ref. 32. These simulations were concerned with formation-keeping and the relative attitude alignment. The relative attitude alignment of the microsatellites was derived by finding the relative attitude of each microsatellite in the inertial frame.[32] Wang and Hadaegh also decoupled the orbital errors from the attitude errors. The decoupling or neglecting the orbital dynamics of the spacecraft is seen in the literature. In most of the literature, the orbital dynamics are neglected because the attitude dynamics occur at a much faster rate than the orbital dynamics. Spacecraft formation flying leads to the modeling of the attitude and orbital dynamics together.

Fragopoulus and Innocenti decoupled the dynamics to derive two controllers and then combined the controllers to control the relative motion between two spacecraft in Ref. 33. The control law utilizes eight thrusters for both the orbital and attitude control. The orbital controller depends on the attitude controller only to determine which thrusters to fire. The attitude controller compensates for the torque applied to the spacecraft by the thruster firing required for the orbital maneuver.[33]

Philip and Ananthasayannam presented a linear coupled attitude and orbital control system using a vision system for the final stage of docking between two spacecraft.[34] The vision system determines the relative position and attitude which allows for the controller to control the spacecraft depending on the relative position rates. Kruep developed a method for computing the minimum fuel trajectory between different satellite positions and orientations.[35] Kruep derived a six-degree-of-freedom optimal trajectory using the linearized Hill-Clohessy-Wiltshire equations and Euler's equations of rigid body motion. This method does not take into account the required attitude maneuvers needed before the thrust is applied to the spacecraft. Pan and Kapilia presented a coupled nonlinear controller to match the attitude of two spacecraft flying in formation.[36] This control law worked well for formation keeping and attitude matching between the spacecraft, but it did not include the attitude maneuvers required for formation keeping. Yamaanaka also ignored these attitude maneuvers in Ref. 37. Yamaanaka developed a feedback control law for attitude control and a feedback and feed-forward orbital control to cancel the relative accelerations between two spacecraft due to orbital motion.

Redding *et al.* derived a linear coupled controller for the Space Shuttle.[38] They discussed having to perform attitude maneuvers to align the orbital maneuvering thrusters, but their model only included a two burn trajectory. This inclusion of the attitude maneuvers is a step in the right direction, which was continued in Ref. 39. Naasz *et al.* discussed and performed simulations of an orbital feedback control law and a magnetic torque coil attitude control system for a spacecraft with limited thruster configurations and power constraints.[39] They applied the control laws to the Virginia Tech Ionospheric Scintillation Measurement Mission, which is part of the Ionospheric Observation Nanosatellite Formation (ION-F) project.[39] The ION-F project will perform formation flying demonstrations while collecting scientific measurements. The orbital feedback control law is presented in Ref. 31 and the attitude control system is described in Refs. 40 and 41. This type of coupling is the direction that coupled control systems for formation flying should head. Further research is required before a coupled attitude and orbital control system can be used for formation flying missions.

2.5 Spacecraft Simulators

The coupled attitude and orbital control system needs to be incorporated into Virginia Tech's Distributed Spacecraft Attitude Control System Simulator (DSACSS). The

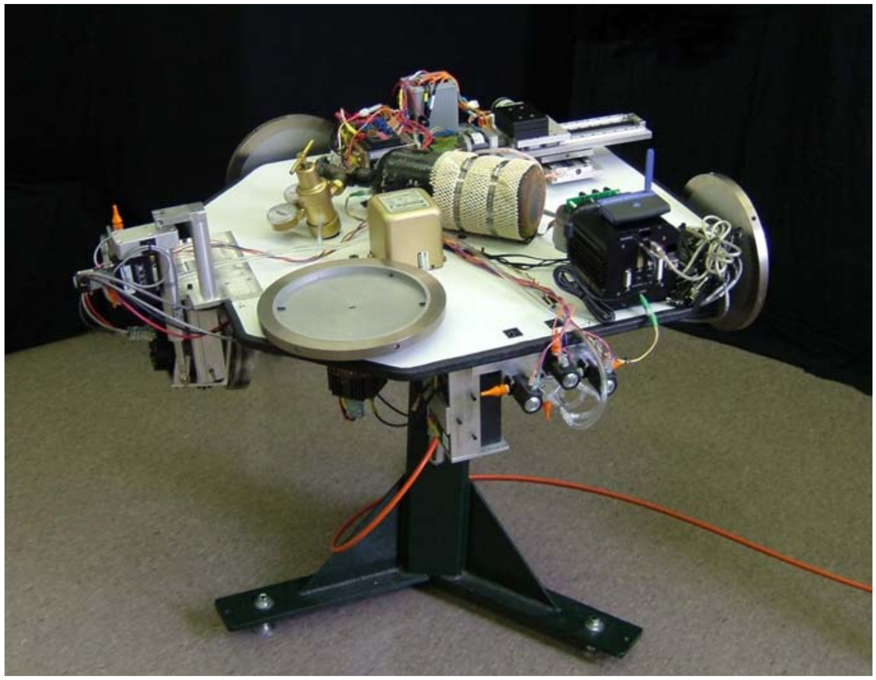

Figure 2.1: Virginia Tech's Whorl-I

DSACSS system is made up of two independent spherical air-bearing platforms for formation flying attitude simulation.[9] Air-bearing platforms have been used for spacecraft simulators for the last 45 years.[42] Air-bearing platforms provide a testbed for attitude controllers, attitude determinations systems, hardware verification and software development for spacecraft.

The DSACSS system is comprised of one tabletop- and one dumbbell-style platforms. The tabletop system is dubbed "Whorl-I" and the dumbbell system is dubbed "Whorl-II." Both systems use identical hardware components except for the structural components.[9] Whorl-I is shown in Figure 2.1 and Whorl-II is shown in Figure 2.2.

The simulators are controlled using an onboard PC/104+ form-factor computer. Each simulator is connected to a wireless network located in the Space Systems Simulation Lab. An external desktop is also connected to the wireless network as the user's access to the simulators. The basic attitude actuators on the simulators are three-axis reaction/momentum wheels (0.075 kg·m^2) and three-axis nitrogen gas thrusters. Whorl-I also has a control moment gyro to perform attitude maneuvers. Attitude determination is currently being performed using three-axis accelerometers and rate gyros. Plans are in the process to add another attitude sensor to allow for complete attitude determination.[9]

The coupled attitude and orbital controller will be implemented using Whorl-I. All of

Figure 2.2: Virginia Tech's Whorl-II

the simulations presented in this thesis are based on the physical properties of Whorl-I. The moments of inertia for Whorl-I are presented in Table 2.1. These values were found using a computer aided design (CAD) model of Whorl-I.

Table 2.1: Whorl-I moment of inertia estimates from CAD model

Parameter	Estimate
I_{xx}	6.2 kg·m^2
I_{xy}	-0.9 kg·m^2
I_{xz}	-0.2 kg·m^2
I_{yy}	7.5 kg·m^2
I_{yz}	0.1 kg·m^2
I_{zz}	12.1 kg·m^2

2.6 Summary

In this chapter we have presented some of the possible applications for the coupled attitude and orbital control system. We have also presented a literature review of attitude, orbital and coupled attitude and orbital controllers developed for formation flying applications. We concluded this chapter by briefly describing Virginia Tech's Distributed Spacecraft Attitude Control System Simulator. We discuss the governing attitude kinematics and dynamics and the orbital dynamics for the coupled control system in Chapter 3.

Chapter 3

Kinematics and Dynamics

Before we examine the controllers we need to define the kinematics and dynamics of the spacecraft system. We assume that the spacecraft uses a three-axis momentum wheel system with N momentum wheels for attitude control. We also assume that the spacecraft has a propulsion system with a variable thrust thruster and is not constrained by the amount of propellant available to complete orbital maneuvers. In this chapter we discuss the attitude kinematics and dynamics and the associated orbital dynamics. Stereographic

3.1 Attitude Kinematics

There are numerous ways to represent the attitude kinematics of a spacecraft. The simplest attitude representation is in the form of Euler axis ($\hat{\mathbf{e}}$) and Euler angle (Φ), which is derived from Euler's Theorem. Euler's Theorem states that the most general motion of a rigid body with a fixed point is a rotation about a fixed axis. Other attitude representations include Euler angles, Quaternions (or Euler Parameters), Rodrigues Parameters, and Modified Rodrigues Parameters (MRPs).[43] The major problem with these representations are the inherent rotation singularities. The choice of which attitude representation to use is dependent on the application and the user preferences.

We describe the kinematics of the spacecraft using Modified Rodrigues Parameters (MRPs).[43] These kinematics are defined by Shuster in Ref. 44. Modified Rodrigues Parameters are defined as

$$\boldsymbol{\sigma} = \hat{\mathbf{e}} \tan\left(\frac{\Phi}{4}\right) \tag{3.1}$$

where $\hat{\mathbf{e}}$ is the Euler axis and Φ is the Euler angle.[43] The MRP singularities occur when $\Phi = l360°$ where l is an integer. We can avoid this singularity by using the MRP shadow set ($\boldsymbol{\sigma}^s$),[45] which is defined as

$$\boldsymbol{\sigma}^s \quad = \quad \frac{1}{\boldsymbol{\sigma}^\mathsf{T}\boldsymbol{\sigma}}\boldsymbol{\sigma} \tag{3.2}$$

The shadow set of MRPs replaces the original MRP set when $\boldsymbol{\sigma}^\mathsf{T}\boldsymbol{\sigma} > 1$. The relationship between the MRPs and the rotation matrix R is

$$R \quad = \quad I_3 + \frac{8\left[\boldsymbol{\sigma}\times\right]\left[\boldsymbol{\sigma}\times\right] - 4\left(1 - \boldsymbol{\sigma}^\mathsf{T}\boldsymbol{\sigma}\right)\left[\boldsymbol{\sigma}\times\right]}{\left(1 + \boldsymbol{\sigma}^\mathsf{T}\boldsymbol{\sigma}\right)^2} \tag{3.3}$$

where I_3 is the 3×3 identity matrix, $[\boldsymbol{\sigma}\times]$ is the skew symmetric matrix defined as

$$[\boldsymbol{\sigma}\times] \quad = \quad \begin{bmatrix} 0 & -\sigma_3 & \sigma_2 \\ \sigma_3 & 0 & -\sigma_1 \\ -\sigma_2 & \sigma_1 & 0 \end{bmatrix} \tag{3.4}$$

and σ_1, σ_2, and σ_3 are the components of $\boldsymbol{\sigma}$. We can also define the kinematic differential equations using MRPs as

$$\dot{\boldsymbol{\sigma}} \quad = \quad G\left(\boldsymbol{\sigma}\right)\boldsymbol{\omega} \tag{3.5}$$

where

$$G\left(\boldsymbol{\sigma}\right) = \frac{1}{2}\left(I_3 + \left[\boldsymbol{\sigma}\times\right] + \boldsymbol{\sigma}\boldsymbol{\sigma}^T - \frac{1 + \boldsymbol{\sigma}^T\boldsymbol{\sigma}}{2}I_3\right) \tag{3.6}$$

and I_3 is the 3×3 identity matrix. The differential equation for the error kinematics is

$$\boldsymbol{\delta}\dot{\boldsymbol{\sigma}} = G\left(\boldsymbol{\delta\sigma}\right)\boldsymbol{\delta\omega} \tag{3.7}$$

where $\boldsymbol{\delta\sigma}$ is the rotational error between the desired attitude and the current attitude of the spacecraft, and $\boldsymbol{\delta\omega}$ is the difference in the angular velocities of the desired attitude and the current attitude found using

$$\boldsymbol{\delta\omega} = \boldsymbol{\omega}_c - R^{cd}\boldsymbol{\omega}_d \tag{3.8}$$

where $\boldsymbol{\omega}_c$ is the actual angular velocity of the spacecraft, $\boldsymbol{\omega}_d$ is the desired angular velocity of the spacecraft, and R^{cd} is the rotation between the actual and desired attitude of the spacecraft.[17]

3.2 Attitude Dynamics

The rotational dynamics of the spacecraft with three-axis control using N momentum wheels is defined in Ref. 17. The dynamics of the system is described as

$$\dot{\mathbf{h}}_B = [\mathbf{h}_B \times] J^{-1} (\mathbf{h}_B - A\mathbf{h}_a) + \mathbf{g}_e \tag{3.9}$$

$$\dot{\mathbf{h}}_a = \mathbf{g}_a \tag{3.10}$$

$$\mathbf{h}_B = I\boldsymbol{\omega}_B + AI_s\boldsymbol{\omega}_s \tag{3.11}$$

where $\mathbf{h}_B$ is the system angular momentum vector, I is the 3×3 moment of inertia matrix of the entire spacecraft, I_s is the $N \times N$ axial moment of inertia matrix, A is the $3 \times N$ matrix containing the axial unit vectors of the momentum wheels, $\mathbf{h}_a$ is the $N \times 1$ matrix of the axial angular momenta of the wheels, $\mathbf{g}_e$ is the 3×1 matrix of the external torques applied to the spacecraft, $\mathbf{g}_a$ is the $N \times 1$ matrix of the internal torques applied to momentum wheels, $\boldsymbol{\omega}_B$ is the 3×1 angular velocity matrix of the body frame expressed in the inertial frame, $\boldsymbol{\omega}_s$ is the $N \times 1$ axial angular velocity matrix of the momentum wheels with respect to the body, and J is the positive definite inertia-like matrix defined as

$$J = I - AI_sA^{\mathsf{T}} \tag{3.12}$$

We define $\boldsymbol{\omega}_B$ and $\mathbf{h}_a$ using equations (3.11) and (3.12)

$$\boldsymbol{\omega}_B = J^{-1} (\mathbf{h}_B - A\mathbf{h}_a) \tag{3.13}$$

$$\mathbf{h}_a = I_sA^{\mathsf{T}}\boldsymbol{\omega}_B + I_s\boldsymbol{\omega}_s \tag{3.14}$$

With the relevant attitude kinematics and dynamics defined, we define the orbital dynamics of the system.

3.3 Orbital Dynamics

The orbital dynamics of spacecraft are most commonly expressed by two-body motion in a gravitational field. The two-body motion allows for perturbation forces to be modeled in the equations of motion. We define the spacecraft motion in the following sections.

3.3.1 Reference Frames

There are numerous reference frames available to describe the motion of the spacecraft. We use the standard Earth-centered inertial, the spacecraft orbital, the Hill, and the

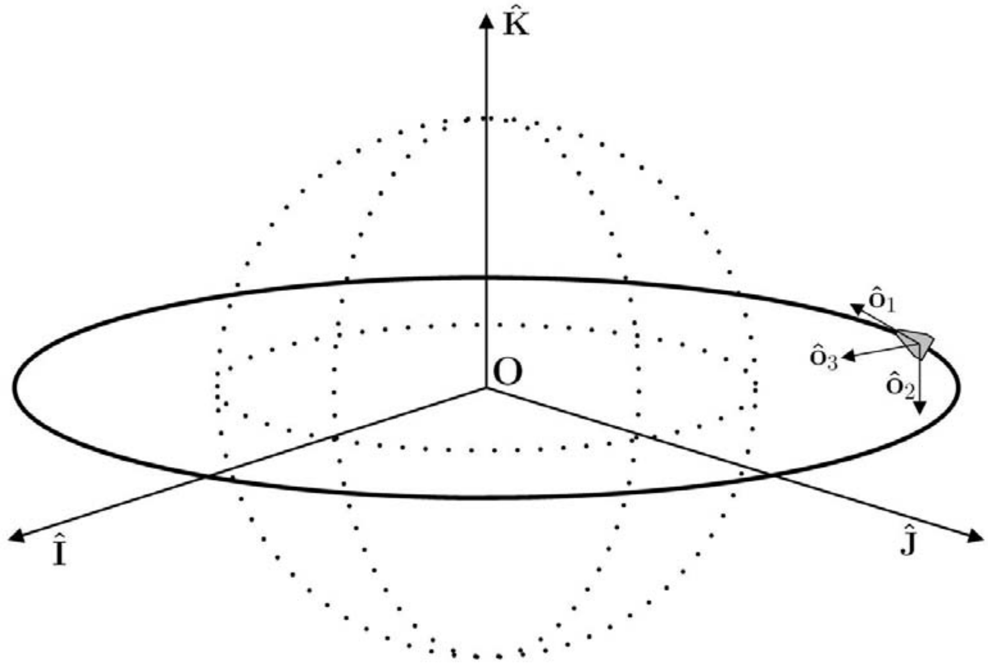

Figure 3.1: The Earth inertial frame and the orbital frame for an equatorial orbit.

spacecraft body-fixed reference frames. The Earth-centered inertial frame has the unit vectors of $\hat{\mathbf{I}}$, $\hat{\mathbf{J}}$, and $\hat{\mathbf{K}}$ with the origin at the center of the Earth, $\mathbf{O}$. The $\hat{\mathbf{I}}$ unit vector is in the vernal equinox direction, the $\hat{\mathbf{I}}$ $\hat{\mathbf{J}}$ plane is defined as the Earth's equatorial plane, and the $\hat{\mathbf{K}}$ direction is defined to be the Earth's spin axis. The spacecraft orbital frame is a rotating reference frame centered at the spacecraft center of mass with unit vectors $\hat{\mathbf{o}}_1$, $\hat{\mathbf{o}}_3$, and $\hat{\mathbf{o}}_3$; where $\hat{\mathbf{o}}_3$ points in the nadir direction, $\hat{\mathbf{o}}_2$ is in the negative orbit normal direction and $\hat{\mathbf{o}}_1$ completes the right-handed coordinate system. If the orbit is circular, then the $\hat{\mathbf{o}}_1$ direction is the velocity direction of the spacecraft.[46] The Earth-centered inertial and the spacecraft orbital frame are shown in Figures 3.1 and 3.2. Figure 3.1 shows the orbital frame of an equatorial orbit and Figure 3.2 shows the orbital frame of a spacecraft in an inclined orbit.

The Hill frame is a relative orbit frame that is used to define the relative motion between spacecraft. The Hill frame defines a chief satellite and deputy satellites, with the reference frame centered at the center of mass of the chief satellite. The position of the deputy satellites is defined relative to the chief satellite. The Hill frame is defined by the unit vectors $\hat{\mathbf{o}}_r$, $\hat{\mathbf{o}}_\theta$, and $\hat{\mathbf{o}}_h$; where $\hat{\mathbf{o}}_r$ is in the orbit radius direction and $\hat{\mathbf{o}}_h$ is in the orbit normal direction of the chief spacecraft. The $\hat{\mathbf{o}}_\theta$ vector completes the right-handed coordinate frame. The Hill frame is shown in Figure 3.3 where the chief satellite is the gray spacecraft and the deputy is the white spacecraft. The variables x, y, and z are the

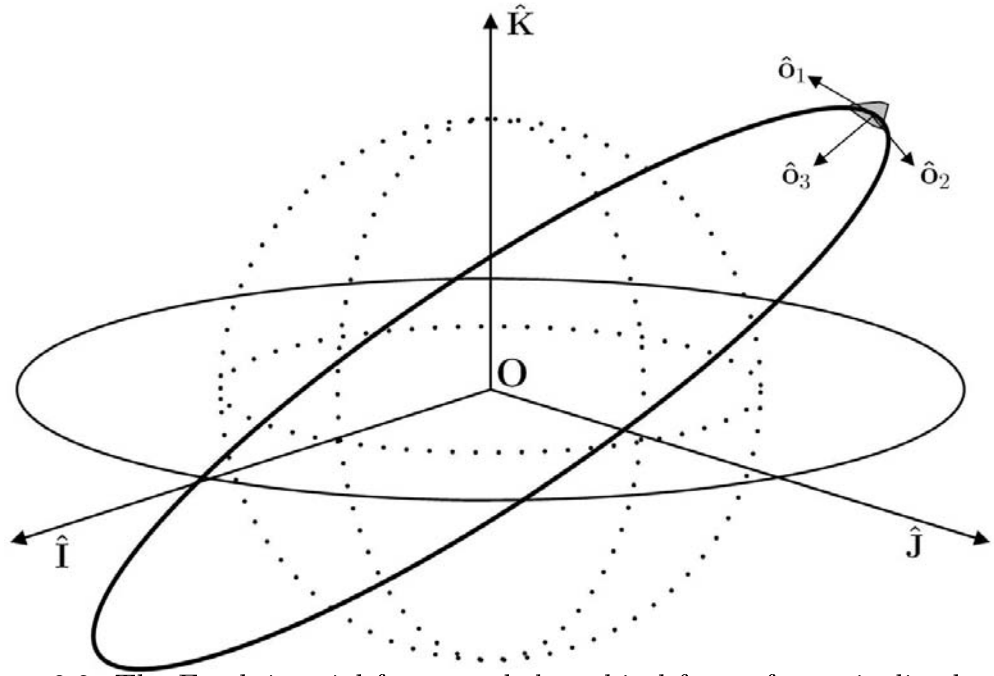

Figure 3.2: The Earth inertial frame and the orbital frame for an inclined orbit.

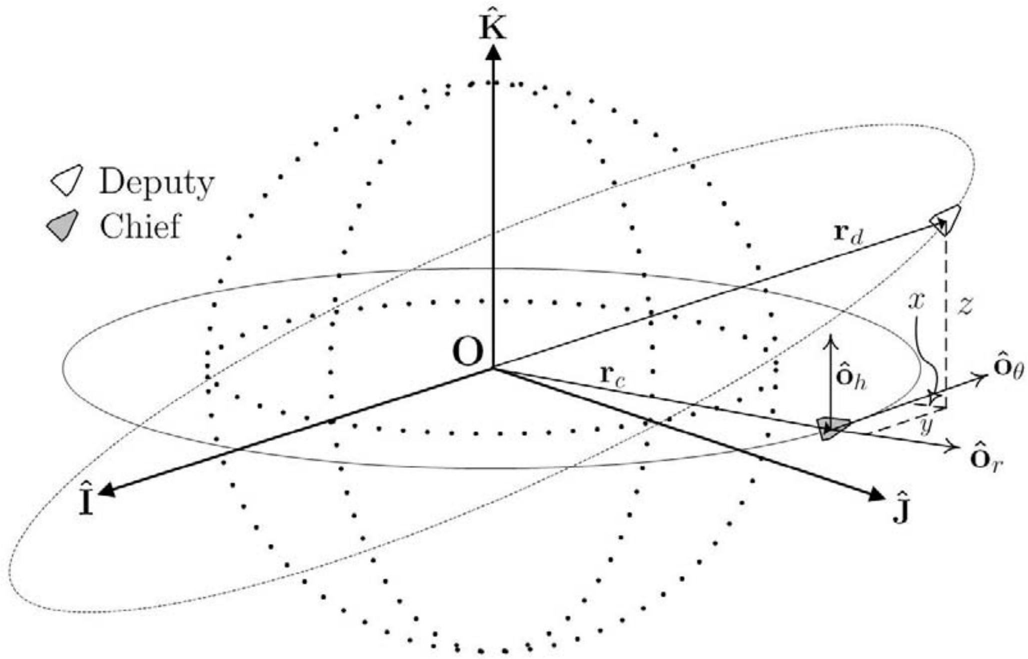

Figure 3.3: The Hill reference frame.

distances in the $\hat{\mathbf{o}}_r$, $\hat{\mathbf{o}}_\theta$, and $\hat{\mathbf{o}}_h$ directions respectively.[43] The body-fixed reference frame of the spacecraft is a right-handed orthogonal coordinate system where the center is the mass center of the spacecraft and the unit vectors are fixed with respect to the spacecraft physical properties.

3.3.2 Cartesian Coordinates

The equations of motion for a point-mass satellite expressed in cartesian coordinates are

$$\ddot{\mathbf{r}} = -\frac{\mu}{\|\mathbf{r}\|^3}\mathbf{r} + \mathbf{a}_p \tag{3.15}$$

where $\mathbf{r}$ is the position vector from the mass center of the primary body to the satellite, μ is the gravitational parameter, and $\mathbf{a}_p$ is the acceleration due to perturbations. If $\mathbf{a}_p = \mathbf{0}$ then we obtain the ideal two-body Keplerian equations of motion about a point-mass central body.

3.3.3 Classical Orbital Elements

Six pieces of information are required to define an orbit and the spacecraft position in that orbit. The simplest form of this information are the components of the spacecraft position and velocity vectors. It is difficult to visualize an orbit given the components of the position and velocity vectors, so we also describe an orbit using the classical orbital elements of the spacecraft. We use the classical orbital elements that are defined as: a is the semi-major axis, e is the eccentricity, i is the inclination, Ω is the right ascension of the ascending node, ω is the argument of periapse, and ν is the true anomaly of the spacecraft.[47]

Using the orbital elements and assuming that the accelerations due to the perturbations are zero, we write the spacecraft orbital equations of motion in Gauss' form of Lagrange's planetary equations[48]

$$\frac{da}{dt} = \frac{2a^2}{h}\left(e\sin\nu u_r + \frac{p}{r}u_\theta\right) \tag{3.16}$$

$$\frac{de}{dt} = \frac{1}{h}\left(p\sin\nu u_r + \left[(p+r)\cos\nu + re\right]u_\theta\right) \tag{3.17}$$

$$\frac{di}{dt} = \frac{r\cos\theta}{h}u_h \tag{3.18}$$

$$\frac{d\Omega}{dt} = \frac{r\sin\theta}{h\sin i}u_h \tag{3.19}$$

$$\frac{d\omega}{dt} = \frac{1}{he}\left[-p\cos\nu u_r + (p+r)\sin\nu u_\theta\right] - \frac{r\sin\theta\cos i}{h\sin i} \tag{3.20}$$

$$\frac{dM}{dt} = n + \frac{b}{ahe}\left[(p\cos\nu - 2re)u_r - (p+r)\sin\nu u_\theta\right] \tag{3.21}$$

where M is the mean anomaly, $\theta = \omega + \nu$ is the argument of latitude, n is the mean motion, p is the semi-latus rectum, h is the angular momentum, b is the semi-minor axis, and u_r, u_θ, and u_h are the radial, transverse, and orbit normal control accelerations. The mean motion for the orbit is defined as

$$n = \sqrt{\frac{\mu}{a^3}} \tag{3.22}$$

where μ is the gravitational parameter for the central body.

3.3.4 Formation Flying

In this thesis we develop the coupled orbit and attitude control system for the use of formation flying spacecraft. For all formation flying spacecraft, we can simplify the model down to the current position of the spacecraft and the desired position of the spacecraft. This is the rendezvous model where the current position spacecraft is the "rendezvous" spacecraft and the desired position is the "target" spacecraft. The coupled system is developed to solve this rendezvous problem. In the numerical simulations, we examine the case where the rendezvous and target spacecraft are in the same orbit with difference in the true anomaly ($\delta\nu$). This orientation is called the leader-follower formation and is shown in Figure 3.4, where the white triangle is the rendezvous spacecraft and the gray triangle is the target spacecraft.

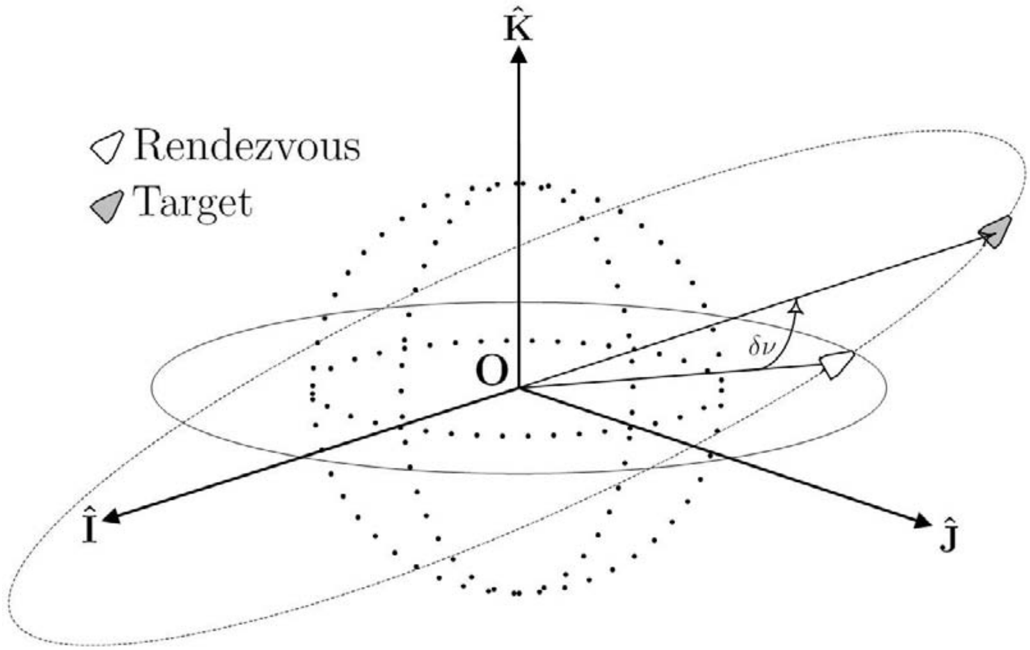

Figure 3.4: The rendezvous and target spacecraft in the leader-follower formation

3.4 Summary

We have introduced the attitude kinematics and dynamics and the orbital dynamics of a spacecraft with three-axis momentum wheel control. We have discussed the different reference frames and the concept of spacecraft formation flying that are used to develop the coupled system. In the next chapter we use the kinematics and dynamics of the system to develop the attitude and orbital control laws.

Chapter 4

Controllers

The coupled attitude and orbital control system uses a nonlinear Lyapunov attitude controller and a nonlinear Lyapunov-based feedback orbital controller as the main parts of the coupled system. The nonlinear attitude controller uses a linear bang-bang attitude controller to initially estimate the required maneuver time for the nonlinear controller. Classical orbital elements are used to develop the Lyapunov-based orbital controller, which is augmented by the addition of a mean motion control strategy. In this chapter we introduce the linear and nonlinear attitude controllers and the orbital controller with the mean motion control strategy.

4.1 Attitude Controllers

The linear and nonlinear attitude controllers are presented in the following section. We derive the linear bang-bang controller and we present the nonlinear attitude controller that was developed in Ref. 17.

4.1.1 Linear (Bang-Bang)

The bang-bang attitude controller provides an estimate of the time required for the nonlinear attitude controller to complete the attitude maneuver. The bang-bang controller is derived using Euler's Law[46]

$$\dot{\mathbf{h}} = \mathbf{g} \tag{4.1}$$

where **h** is the angular momentum about the mass center of the system and **g** is the net applied moment about the mass center. We constrain the problem to be a planar problem which leads to

$$\begin{aligned} \dot{h} &= g \\ I_{\max}\ddot{\phi} &= g_{\max} \end{aligned} \tag{4.2}$$

where $I_{\max}$ is the maximum moment of inertia of the system, $\ddot{\phi}$ is the angular acceleration about the major axis, and $g_{\max}$ is the maximum applied torque that momentum wheels can produce on the system. Integrating Equation (4.2) twice, we obtain

$$\begin{aligned} \int_{\dot{\phi}_o}^{\dot{\phi}} I_{\max} d\dot{\phi} &= \int_{t_o}^{t} g_{\max} dt \\ I_{\max}\left(\dot{\phi} - \dot{\phi}_o\right) &= g_{\max}\left(t - t_o\right) \qquad (4.3) \\ \int_{\phi_o}^{\phi} I_{\max} d\phi &= \int_{t_o}^{t}\left(g_{\max}\Delta t + I_{\max}\dot{\phi}_o\right) dt \\ I_{\max}\Delta\phi &= g_{\max}\left(\frac{\Delta t^2}{2} - t_o\Delta t\right) + I_{\max}\dot{\phi}_o\left(\Delta t\right) \qquad (4.4) \end{aligned}$$

where $\Delta\phi = \phi - \phi_o$ and $\Delta t = t - t_o$. We define $t_o = 0$ and obtain

$$I_{\max}\Delta\phi = \frac{1}{2} g_{\max}\Delta t^2 + I_{\max}\dot{\phi}_o\Delta t \tag{4.5}$$

We assume that $\dot{\phi}_o = 0$, $\phi_o = 0$, and $\dot{\phi}$ is defined as a ramp function where the positive maximum torque is applied for the first half of the maneuver and the negative maximum torque is applied for the second half of the maneuver.[49] This ramp function leads us to examine the first half of the maneuver, where

$$I_{\max}\left(\phi - \frac{\phi}{2}\right) = \frac{1}{2} g_{\max}\left(\frac{\Delta t}{2}\right)^2 \tag{4.6}$$

Solving equation (4.6) for Δt produces

$$\Delta t = 2\sqrt{\frac{2I_{\max}}{g_{\max}}\left(\phi - \frac{\phi}{2}\right)} \tag{4.7}$$

Equation (4.7) provides the estimate of time that is required to complete an attitude maneuver using the nonlinear controller.

4.1.2 Nonlinear

The nonlinear Lyapunov attitude controller is presented in Ref. 17 with the following candidate Lyapunov function:

$$V = \frac{1}{2}\boldsymbol{\delta\omega}^{\mathsf{T}} K \boldsymbol{\delta\omega} + 2k_1 \ln(1 + \boldsymbol{\delta\sigma}^{\mathsf{T}}\boldsymbol{\delta\sigma}) \tag{4.8}$$

where $K = K^{\mathsf{T}} > 0$, $\boldsymbol{\delta\omega}$ is the angular velocity error, $\boldsymbol{\delta\sigma}$ is the rotation error between the desired and current attitude states, and $k_1 > 0$. After differentiating Equation (4.8) and some simplification

$$\dot{V} = \boldsymbol{\delta\omega}^{\mathsf{T}} \left[[\mathbf{h}_B \times] J^{-1} (\mathbf{h}_B - A\mathbf{h}_a) + \mathbf{g}_e - A\mathbf{g}_a + k_1 \boldsymbol{\delta\sigma} \right]$$

where $\mathbf{h}_B$ is the system angular momentum vector, J is the inertia-like matrix defined in Equation (3.12), A is the matrix containing the axial unit vectors of the momentum wheels, $\mathbf{h}_a$ is the matrix of axial angular momenta of the wheels, $\mathbf{g}_e$ are the external torques applied to the spacecraft, and $\mathbf{g}_a$ are the internal torques applied to the momentum wheels. The external torques and internal torques that are chosen to make $\dot{V}$ negative semi-definite and bounded

$$\begin{aligned} \mathbf{g}_e &= \mathbf{0} \\ \mathbf{g}_a &= A^{-1} \left[[\mathbf{h}_B \times] J^{-1} (\mathbf{h}_B - A\mathbf{h}_a) + \mathbf{g}_e + k_1 \boldsymbol{\delta\sigma} + k_2 \boldsymbol{\delta\omega} \right] \end{aligned} \tag{4.9}$$

where $k_2 > 0$. Plugging Equation (4.9) into Equation (4.9), $\dot{V}$ simplifies to

$$\dot{V} = -k_2 \boldsymbol{\delta\omega}^T \boldsymbol{\delta\omega} \tag{4.10}$$

LaSalle's Theorem[50] was used to prove that $\dot{V}$ is negative-definite. Proving $\dot{V}$ is negative-definite leads to the conclusion that the error dynamics and kinematics with the feedback control law in Equation (4.9) is globally asymptotically stable.

4.1.3 Gain Selection

The gains (k_1 and k_2) for the nonlinear attitude controller are constrained to be positive for a globally asymptotically stable control law. The gains are chosen dependent on amount of torque available for attitude maneuvers and how aggressively the angular velocity is to be damped.

We have presented the linear and nonlinear attitude controllers for a spacecraft with three-axis control using N momentum wheels. We present the classical orbital element control law and mean motion control strategy in the next section.

4.2 Orbital Controllers

The nonlinear Lyapunov-based classical orbital element control law and mean motion control strategy were developed in Ref. 31. The classical orbital element control law and mean motion control strategy are presented in the following sections.

4.2.1 Classical Orbital Element

Recall Gauss' form of the Lagrange's planetary equations,[48] Equations (3.16)–(3.21)

$$
\begin{aligned}
\frac{da}{dt} &= \frac{2a^2}{h}\left(e\sin\nu u_r + \frac{p}{r}u_\theta\right) \\
\frac{de}{dt} &= \frac{1}{h}\left(p\sin\nu u_r + \left[(p+r)\cos\nu + re\right]u_\theta\right) \\
\frac{di}{dt} &= \frac{r\cos\theta}{h}u_h \\
\frac{d\Omega}{dt} &= \frac{r\sin\theta}{h\sin i}u_h \\
\frac{d\omega}{dt} &= \frac{1}{he}\left[-p\cos\nu u_r + (p+r)\sin\nu u_\theta\right] - \frac{r\sin\theta\cos i}{h\sin i} \\
\frac{dM}{dt} &= n + \frac{b}{ahe}\left[(p\cos\nu - 2re)u_r - (p+r)\sin\nu u_\theta\right]
\end{aligned}
$$

where a is the semi-major axis, e is the eccentricity, i is the inclination, Ω is the right ascension of the ascending node, ω is the argument of periapse, M is the mean anomaly, ν is the true anomaly, θ is the argument of latitude, n is the mean motion, p is the semi-latus rectum, h is the angular momentum, b is the semi-minor axis, and u_r, u_θ, and u_h are the radial, transverse, and orbit normal control accelerations. Equations (3.16)–(3.21) are rewritten in the following form

$$\dot{\text{œ}} = \mathbf{f}(\text{œ}) + \tilde{H}(\text{œ})\,\mathbf{u} \tag{4.11}$$

where **œ** is the vector of orbital elements, $[a\ e\ i\ \Omega\ \omega\ M]^\mathsf{T}$, $\tilde{H}(\text{œ})$ is the input matrix found using Equations (3.16–3.21), and $\mathbf{u}$ is the vector of controls $[u_r\ u_\theta\ u_h]^\mathsf{T}$. The equations of motion for the first five orbital elements are redefined as

$$\dot{\boldsymbol{\eta}} = H\mathbf{u} \tag{4.12}$$

where

$$\boldsymbol{\eta} = \begin{bmatrix} a - a^* \\ e - e^* \\ i - i^* \\ \Omega - \Omega^* \\ \omega - \omega^* \end{bmatrix} = \begin{bmatrix} \delta a \\ \delta e \\ \delta i \\ \delta\Omega \\ \delta\omega \end{bmatrix} \tag{4.13}$$

where $(\cdot)^*$ is the target element and

$$H = \begin{bmatrix} \frac{2a^2 e \sin\nu}{h} & \frac{2a^2 p}{hr} & 0 \\ \frac{p\sin\nu}{h} & \frac{(p+r)\cos\nu + re}{h} & 0 \\ 0 & 0 & \frac{r\cos(\omega+\nu)}{h} \\ 0 & 0 & \frac{r\sin(\omega+\nu)}{h\sin i} \\ -\frac{p\cos\nu}{he} & \frac{(p+r)\sin\nu}{he} & -\frac{r\sin(\omega+\nu)\cos i}{h\sin i} \end{bmatrix} \tag{4.14}$$

The control law was developed using a quadratic, positive definite Lyapunov function, and was proved that the control law is globally asymptotically stable. The control law for the first five orbital elements is

$$\mathbf{u} \;=\; -H^{\mathsf{T}}\tilde{K}\boldsymbol{\eta} = -\begin{bmatrix} \frac{2a^2 e \sin\nu}{h} & \frac{2a^2 p}{hr} & 0 \\ \frac{p\sin\nu}{h} & \frac{(p+r)\cos\nu + re}{h} & 0 \\ 0 & 0 & \frac{r\cos(\omega+\nu)}{h} \\ 0 & 0 & \frac{r\sin(\omega+\nu)}{h\sin i} \\ -\frac{p\cos\nu}{he} & \frac{(p+r)\sin\nu}{he} & -\frac{r\sin(\omega+\nu)\cos i}{h\sin i} \end{bmatrix}^{\mathsf{T}} \begin{bmatrix} K_a\delta a \\ K_e\delta e \\ K_i\delta i \\ K_\Omega\delta\Omega \\ K\omega\delta\omega \end{bmatrix} \tag{4.15}$$

where K_a, K_e, K_i, K_Ω, and K_ω are positive gains. The angle errors $\delta\Omega$ and $\delta\omega$ are defined between $-\pi$ and π.

4.2.2 Mean Motion

The mean motion control is accomplished by defining a new target semi-major axis, a^{**}, which forces the mean anomaly error to zero[31]

$$a^{**} \;=\; \left(-K_n\delta M + \frac{1}{a^{*3/2}}\right)^{-2/3} \tag{4.16}$$

Here K_n is a positive gain and δM is defined between $-\pi$ and π. As δM goes to zero, we regain the original target semi-major axis, a^*. Naasz and Hall recommended replacing δM with $\delta\theta$ in application, so that the mean motion control properly positions the spacecraft within the orbital plane for circular orbits.[31]

4.2.3 Gain Selection

Naasz and Hall also developed a gain selection method in Ref. 31. The gains for the classical orbital element controller are found using

$$K_a = \frac{h^2}{4a^2(1+e)^2}\frac{1}{\Delta t_t} \tag{4.17}$$

$$K_e = \frac{h^2}{4p^2}\frac{1}{\Delta t_t} \tag{4.18}$$

$$K_i = \left[\frac{h + eh\cos\left(\omega + \sin^{-1} e\sin\omega\right)}{p\left(-1 + e^2\sin^2\omega\right)}\right]^2 \frac{1}{\Delta t_t} \tag{4.19}$$

$$K_\Omega = \left[\frac{h\sin i\left(-1 + e\sin\left(\omega + \sin^{-1} e\cos\omega\right)\right)}{p\left(1 - e^2\cos^2\omega\right)\sqrt{\Delta t_t}}\right]^2 \tag{4.20}$$

$$K_\omega = \frac{e^2h^2}{p^2}\left(1 - \frac{e^2}{4}\right)\frac{1}{\Delta t_t} \tag{4.21}$$

where Δt_t is the length of the thruster firing. The mean motion gain, K_n is chosen depending on how aggressively we want to correct the argument of latitude error.[31] These gains are calculated at the beginning of the orbital maneuver and are held constant for the duration of the maneuver.

4.3 Summary

In this chapter, we have presented the linear attitude controller and the nonlinear attitude controller. The linear control law (Equation (4.7)) is used to estimate the time that the nonlinear controller (Equation (4.9)) will take to perform a maneuver. The orbital controller is presented as a classical orbital element Lyapunov-based control law, Equation (4.15), and a mean motion control strategy, Equation (4.16). The coupled attitude and orbital control system is developed in Chapter 5.

Chapter 5

Coupled System

The coupled attitude and orbital control system is developed using the linear and nonlinear attitude controllers and the orbital controller that were discussed in Chapter 4. The coupled system also requires an orbital propagator and an attitude check method. We define the orbital controller as the "thrust direction estimator" and the orbital propagator as the "orbital estimator" for the use with the coupled system. In this chapter we describe the overall program architecture of the coupled system and define the orbital estimator and the attitude check method.

5.1 Program Architecture

The overall program architecture is shown in Figure 5.1, where each block is a separate function with the specific inputs and outputs shown in the bottom portion of the blocks. The simulation begins by defining a position and velocity of the target ($\mathbf{r}^t_\circ$ and $\mathbf{v}^t_\circ$) and rendezvous ($\mathbf{r}^r_\circ$ and $\mathbf{v}^r_\circ$) spacecraft along with the attitude of the rendezvous spacecraft ($\boldsymbol{\sigma}_\circ$) at the initial time $t_\circ$. These initial conditions are used as the first set of inputs into the control loop. The thrust direction estimator uses the position ($\mathbf{r}^r_\circ$, $\mathbf{r}^t_\circ$) and velocity ($\mathbf{v}^r_\circ$, $\mathbf{v}^t_\circ$) data to produce a desired thrust vector ($\mathbf{T}^{\text{int}}_{\text{ideal}}$) in the inertial frame at $t_\circ$. This desired thrust vector direction and the spacecraft physical properties are used to determine a desired attitude ($\boldsymbol{\sigma}^{\text{int}}$) of the rendezvous spacecraft. The bang-bang attitude controller uses the current attitude ($\boldsymbol{\sigma}_\circ$) of the spacecraft (at $t_\circ$) and the desired attitude to estimate the time to complete the attitude maneuver using the nonlinear attitude controller. This time estimate (Δt_e) is used by the orbital estimator to determine the position ($\mathbf{r}^r_e$, $\mathbf{r}^t_e$) and velocity ($\mathbf{v}^r_e$, $\mathbf{v}^t_e$) of both spacecraft after the attitude maneuver. The estimated position and velocity data after the Δt_e required for the attitude maneuver are used by

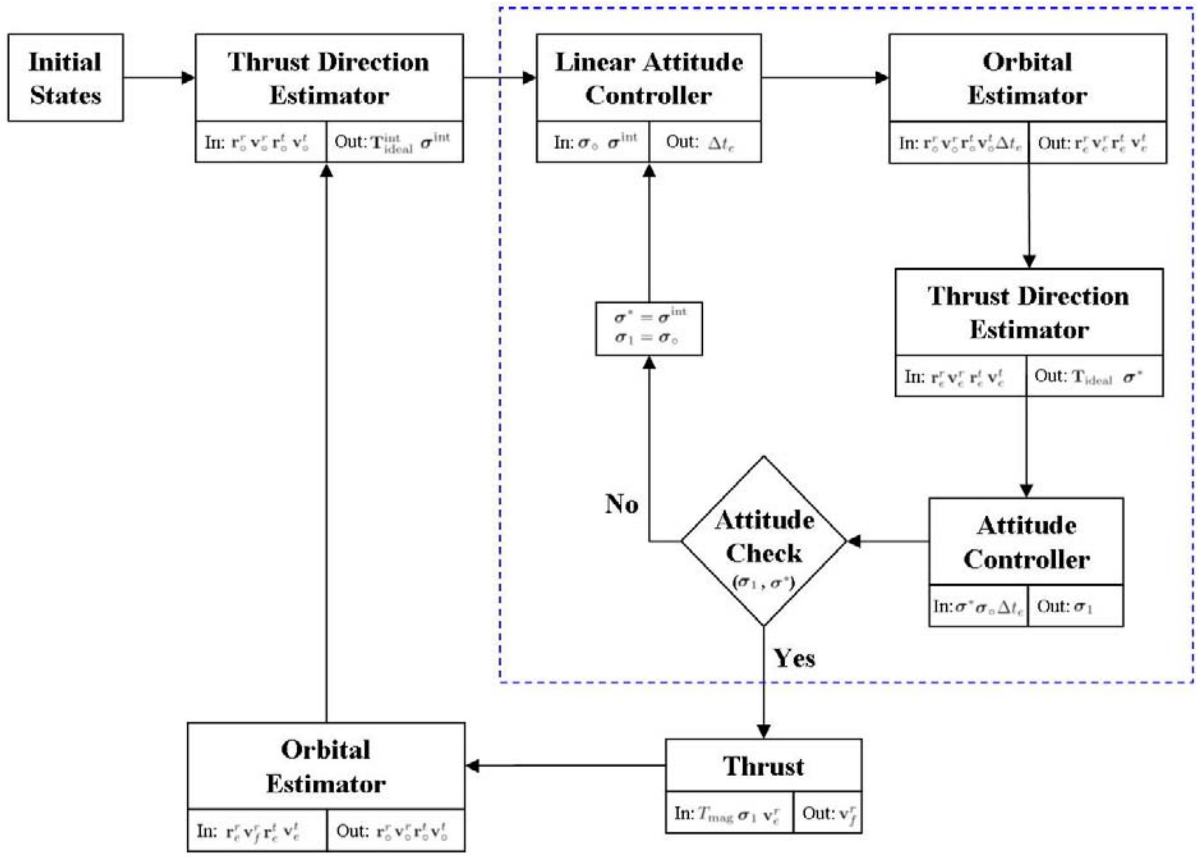

Figure 5.1: The overall simulation architecture

the thrust direction estimator to determine the desired thrust vector ($\mathbf{T}_{\rm ideal}$) after the attitude maneuver (Δt_e). The thrust direction and the spacecraft physical properties are used to determine the desired attitude ($\boldsymbol{\sigma}^*$) after Δt_e. The nonlinear attitude controller uses the attitude ($\boldsymbol{\sigma}_\circ$) of the rendezvous spacecraft at t_o and the desired attitude ($\boldsymbol{\sigma}^*$) after Δt_e as the initial inputs. The nonlinear attitude control maneuver is performed for the duration of time that the linear bang-bang attitude controller estimated (Δt_e).

The current attitude ($\boldsymbol{\sigma}_1$) after Δt_e is compared to the desired attitude ($\boldsymbol{\sigma}^*$) by the attitude check function. This function determines if the current attitude is within a set of error limits that the user specifies. If the current attitude is not within the error limits, then the current attitude and the position and velocity of the target and rendezvous spacecraft are used as the new inputs of the control loop. If the current attitude is within the error limits, then the thruster "fires" according to the current attitude. The thruster is considered an ideal thruster, so the magnitude of the thrust ($T_{\rm mag}$) is variable and is equal to the magnitude of the desired thrust direction vector ($\mathbf{T}_{\rm ideal}$). The thrust is applied to the rendezvous spacecraft in the form of an impulsive Δv over a user-specified time interval (t_2). The orbital estimator uses the thrust time along with the position ($\mathbf{r}_e^r$, $\mathbf{r}_e^t$) and velocity ($\mathbf{v}_f^r$, $\mathbf{v}_e^t$) after the addition of the Δv to determine the position and velocity of the spacecraft at t_2. The position ($\mathbf{r}_\circ^r$, $\mathbf{r}_\circ^t$) and velocity ($\mathbf{v}_\circ^r$, $\mathbf{v}_\circ^t$) at t_2 of both spacecraft and the attitude ($\boldsymbol{\sigma}_1$) of the rendezvous spacecraft are used as the new inputs to the control loop. The user defines the number of orbits to simulate and the control loop keeps track of the total time of the orbital maneuver.

This program architecture is different from previous work where the section inside the dashed bock was assumed to be the attitude maneuver. This simplified program architecture was used by Nassz *et al.* in Ref. 39. Nassz *et al.* did not recalculate the desired thrust direction for the orbital maneuver after the attitude maneuver has been completed. This recalculation is included in the functions inside of the dashed box.

5.2 Orbital Estimator

The orbital estimator is used to propagate the orbits of both the target spacecraft and the rendezvous spacecraft. The orbital estimator is the f and g method which is a solution of Kepler's two-body problem. We use the f and g expressions in terms of eccentric anomaly to propagate the spacecraft orbit.[47] The f and g method requires the input of the initial position ($\mathbf{r}_\circ$) and velocity ($\mathbf{v}_\circ$) vectors of the spacecraft, and the propagation time (Δt). Using the initial position and velocity vectors, we calculate the semi-major axis (a) using the orbital energy equation

$$\mathcal{E} = \frac{v_\circ}{2} - \frac{\mu}{r_\circ} = -\frac{\mu}{2a} \tag{5.1}$$

where $\mathcal{E}$ is the total energy of the orbit, μ is the gravitational parameter, and $r_\circ$ and $v_\circ$ are the magnitudes of the initial position and velocity vectors, respectively. Using the semi-major axis and the initial position and velocity vectors, we find the eccentricity (e) of the orbit using the orbit angular momentum vector ($\mathbf{h}_o$),

$$\mathbf{h}_o = [\mathbf{r}_\circ\times]\mathbf{v}_\circ \tag{5.2}$$

$$h_o = \sqrt{\mu a\,(1-e)} \tag{5.3}$$

where h_o is the magnitude of the orbit angular momentum vector. We find the initial eccentric anomaly ($E_\circ$) using

$$r_\circ = a\,(1 - e\cos E_\circ) \tag{5.4}$$

A quadrant check is required after $E_\circ$ is calculated. This quadrant check is

$$\mathbf{r}_\circ^{\mathrm{T}}\mathbf{v}_\circ > 0 \;\Rightarrow\; 0 < E_\circ < \pi \tag{5.5}$$

$$\mathbf{r}_\circ^{\mathrm{T}}\mathbf{v}_\circ < 0 \;\Rightarrow\; \pi < E_\circ < 2\pi \tag{5.6}$$

Using the initial eccentric anomaly, we can find the initial mean anomaly ($M_\circ$) by

$$M_\circ = E_\circ - e \sin E_\circ \tag{5.7}$$

Propagating the orbit by Δt leads to change in mean anomaly (M_t) and eccentric anomaly (E_t) by

$$\begin{aligned} M_t &= M_\circ + n\Delta t && (5.8) \\ M_t &= E_t - e \sin E_t && (5.9) \end{aligned}$$

where n is the mean motion of the orbit. Equation (5.9 is solved using Newton's method. We find the magnitude of the new position vector using

$$r_t = a\,(1 - e \cos E_t) \tag{5.10}$$

and the change in eccentric anomaly (ΔE) by

$$\Delta E = E_t - E_\circ \tag{5.11}$$

The f and g expressions expressed in terms of eccentric anomaly are[47]

$$\begin{aligned} f_E &= 1 - \frac{a}{r_o}\,(1 - \cos \Delta E) && (5.12) \\ g_E &= \Delta t - \sqrt{\frac{a^3}{\mu}}\,(\Delta E - \sin \Delta E) && (5.13) \\ \dot{f}_E &= -\frac{\sqrt{\mu a}\sin \Delta E}{r_t r_o} && (5.14) \\ \dot{g}_E &= 1 - \frac{a}{r_t}\,(1 - \cos \Delta E) && (5.15) \end{aligned}$$

The final position ($\mathbf{r}_t$) and velocity ($\mathbf{v}_t$) vectors are calculated using[47]

$$\begin{aligned} \mathbf{r}_t &= f_E \mathbf{r}_\circ + g_E \mathbf{v}_\circ && (5.16) \\ \mathbf{v}_t &= \dot{f}_E \mathbf{r}_\circ + \dot{g}_E \mathbf{v}_\circ && (5.17) \end{aligned}$$

The f and g method is an idealized orbital estimator because this method does not include any orbital perturbations.[47]

5.3 Attitude Check

Before the spacecraft can fire the thruster, we need to determine if the spacecraft's attitude is "close enough" to the desired attitude. Comparing the actual attitude and the desired attitude is accomplished by determining the rotation matrix between the two attitudes. We would also like to obtain a simple relationship to calculate the effect of an attitude error before an orbital maneuver is performed.

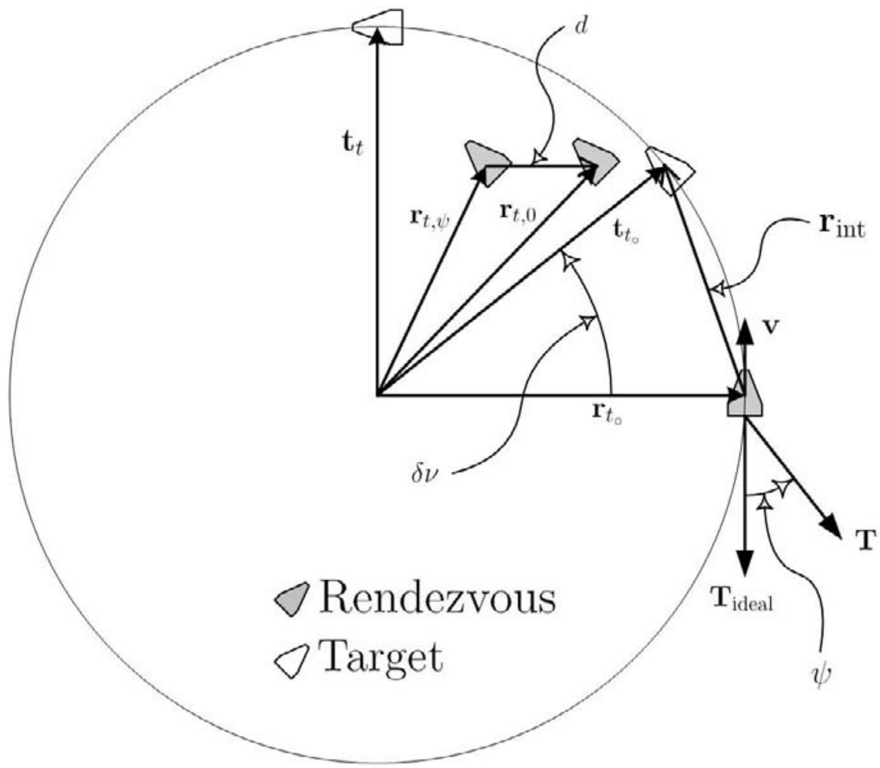

Figure 5.2: Attitude and position error geometry

5.3.1 Approach and Nomenclature

We define some of the nomenclature needed to examine these problems in Figure 5.2. The initial position of the rendezvous and target spacecraft are denoted by $\mathbf{r}_{t_\circ}$ and $\mathbf{t}_{t_\circ}$ respectively. The initial in-track error between the two spacecraft is represented as $\mathbf{r}_{\text{int}}$ or as the difference in the true anomaly $\delta\nu$. The initial velocity direction of the rendezvous spacecraft is denoted by $\mathbf{v}$. These initial conditions are used to determine the ideal thrust vector ($\mathbf{T}_{\text{ideal}}$) using the orbital controller. The thrust vector with an attitude error, $\mathbf{T}$, has the same magnitude (T_{mag}) as $\mathbf{T}_{\text{ideal}}$. We limit the attitude error to only be in the orbital plane, so that the attitude error is represented by the angle ψ. We define ψ to be a positive rotation about the orbit normal direction away from the ideal thrust direction.

To examine the effect of ψ, we apply the ideal thrust vector to the rendezvous spacecraft and propagate the resulting orbit for a duration of time, t. The resulting ideal position is defined as $\mathbf{r}_{t,0}$ in Figure 5.2. We also apply the attitude error thrust vector to the rendezvous spacecraft and propagate the resulting orbit for the same duration of time, t. This resulting position is defined as $\mathbf{r}_{t,\psi}$ in Figure 5.2. The position of the target spacecraft is also propagated using the time t, and the resulting position of the target spacecraft is denoted by $\mathbf{t}_t$. To determine the effect of the attitude error we define the separation distance, d, which is the scalar difference between $\mathbf{r}_{t,0}$ and $\mathbf{r}_{t,\psi}$.

We use an exact solution to the two-body problem and an approximate solution to examine the effect of attitude error on the separation distance. The exact solution is the f and g method and the approximate solution is found using the Hill-Clohessy-Wiltshire relative orbit equations. The following sections introduce the two methods and the corresponding results.

5.3.2 Exact Method

For the attitude error investigation we use the f and g expressions in terms of eccentric anomaly.[47] The f and g method requires the input of the initial position ($\mathbf{r}_{t_\circ}$), and the velocity of the rendezvous spacecraft. The input velocity $\mathbf{v}_i$ is found by adding an impulsive change in velocity to the initial velocity of the rendezvous spacecraft $\mathbf{v}$:

$$\mathbf{v}_i = \mathbf{v} + \mathbf{T}\frac{t_{oc}}{m} \tag{5.18}$$

where

$$\mathbf{T} = R^{io} R^{ad} \mathbf{T}_{\text{ideal}} \tag{5.19}$$

$$\mathbf{T} = R^{io} \begin{bmatrix} \cos(-\psi) & 0 & -\sin(-\psi) \\ 0 & 1 & 0 \\ \sin(-\psi) & 0 & \cos(-\psi) \end{bmatrix} \mathbf{T}_{\text{ideal}} \tag{5.20}$$

Here t_{oc} is the thrust time used by the orbital controller, m is the mass of the rendezvous spacecraft, R^{io} is the rotation between the orbital and inertial frame and R^{ad} is the negative rotation of the attitude error, ψ, about the negative orbit normal direction ($\hat{\mathbf{o}}_2$) away from the ideal thrust direction ($\mathbf{T}_{\text{ideal}}$). The f and g method is used to determine the final position ($\mathbf{r}_{t,\psi}$) and velocity ($\mathbf{v}_{\mathbf{t},\psi}$) vectors. The separation distance, d, is subsequently found by applying the distance formula between the ideal position ($\mathbf{r}_{t,0}$) and the position due to the attitude error ($\mathbf{r}_{t,\psi}$).

5.3.3 Approximate Method

Another way to determine the separation distance is to use the Hill-Clohessy-Wiltshire equations of motion for relative orbits. Recall the Hill-Clohessy-Wiltshire equations of motion represented in the Hill coordinate frame:[43]

$$\ddot{x} - 2n\dot{y} - 3n^2 x = 0 \tag{5.21}$$
$$\ddot{y} + 2n\dot{x} = 0 \tag{5.22}$$
$$\ddot{z} + n^2 z = 0 \tag{5.23}$$

where x is in the radial direction, z is in the orbit normal direction of the reference spacecraft and y is in the direction that completes the right-handed coordinate system. These equations of motion assume that the reference orbit is circular and that the relative position errors are small compared to the orbit radius, which defines the y direction is in the spacecraft velocity direction. We have restricted the attitude error to be in the orbital plane, which allows us to examine the radial and in-track equations of motion, Equations (5.21) and (5.22). Schaub and Junkins (Ref. 43) presented the analytical solution to the Hill-Clohessy-Wiltshire equations of motion as

$$x(t) = A_\circ \cos(nt + \alpha) + x_{\text{off}} \tag{5.24}$$
$$y(t) = -2A_\circ \sin(nt + \alpha) - \frac{3}{2} nt x_{\text{off}} + y_{\text{off}} \tag{5.25}$$

where n is the mean motion of the spacecraft, t is the time, $A_\circ$ and α are constants, and x_{off} and y_{off} are integration constants. Applying the initial relative position and velocity between the two spacecraft, we can determine the constants

$$A_\circ = \frac{(3nx_\circ + 2\dot{y}_\circ)\sqrt{\dot{x}_\circ^2 + (3nx_\circ + 2\dot{y}_\circ)^2}}{n(3nx_\circ + 2\dot{y}_\circ)} \tag{5.26}$$
$$\alpha = -\arccos\left(-\frac{3nx_\circ + 2\dot{y}_\circ}{\sqrt{\dot{x}_\circ^2 + (3nx_\circ + 2\dot{y}_\circ)^2}}\right) \tag{5.27}$$
$$x_{\text{off}} = -\frac{2\dot{x}_\circ}{n} + y_\circ \tag{5.28}$$
$$y_{\text{off}} = 4x_\circ + \frac{2\dot{y}_\circ}{n} \tag{5.29}$$

where $x_\circ$ and $y_\circ$ are the initial relative position and $\dot{x}_\circ$ and $\dot{y}_\circ$ are the initial relative velocity conditions between the two spacecraft in the Hill frame. Determining the relative velocity between the two spacecraft in the Hill frame requires us to account for the rotating reference frame.

To determine the separation distance, d, we use two sets of Equations (5.24) and (5.25) with one set using the ideal initial conditions and the other set using the initial conditions with an attitude error (ψ). Subtracting the two sets of equations we find

$$\Delta x = \frac{(\dot{x}_\circ^e - \dot{x}_\circ^i)\sin nt}{n} + \frac{2(\dot{y}_\circ^e - \dot{y}_\circ^i)(1 - \cos nt)}{n} \tag{5.30}$$
$$\Delta y = \frac{(\dot{y}_\circ^e - \dot{y}_\circ^i)(4\sin nt - 3nt)}{n} + \frac{2(\dot{x}_\circ^e - \dot{x}_\circ^i)(\cos nt - 1)}{n} \tag{5.31}$$

where Δx is the difference between the equations in the x direction in the Hill frame, Δy is the difference between the equations in the y direction in the Hill frame, $\dot{x}_\circ^i$ and $\dot{y}_\circ^i$ are the initial relative velocity for the ideal case and $\dot{x}_\circ^e$ and $\dot{y}_\circ^e$ are the initial relative velocity for the attitude error case. The separation distance, d, is found using

$$d = \sqrt{\Delta x^2 + \Delta y^2} \tag{5.32}$$
$$\tag{5.33}$$

This method determines the separation distance between the ideal case and the case with an attitude error.

5.3.4 Results

The orbit that is used for the attitude error study is defined by the orbital elements in Table 5.1. The exact and approximate solutions are used to examine the separation

Table 5.1: Orbital elements used for attitude error study

Parameter	Estimate	Units
a	6823	km
e	0.001	
i	28	degrees
Ω	135	degrees
ω	90	degrees
ν	45	degrees

distance caused by the attitude error for initial in-track error magnitudes, $\mathbf{r}_{\text{int}}$ in Figure 5.2, of 0.5, 1.0, 1.5, and 2.0 km. The ideal thrust vectors are obtained using the initial in-track error and the orbital controller. The ideal thrust vectors for the different initial in-track error magnitudes are

$$r_{\text{int}} = 0.5\,(\text{km}) \Rightarrow 3.17 \times 10^{-3}\hat{\mathbf{T}} \quad (\text{N}) \tag{5.34}$$
$$r_{\text{int}} = 1.0\,(\text{km}) \Rightarrow 6.34 \times 10^{-3}\hat{\mathbf{T}} \quad (\text{N}) \tag{5.35}$$
$$r_{\text{int}} = 1.5\,(\text{km}) \Rightarrow 9.50 \times 10^{-3}\hat{\mathbf{T}} \quad (\text{N}) \tag{5.36}$$
$$r_{\text{int}} = 2.0\,(\text{km}) \Rightarrow 12.66 \times 10^{-3}\hat{\mathbf{T}} \quad (\text{N}) \tag{5.37}$$

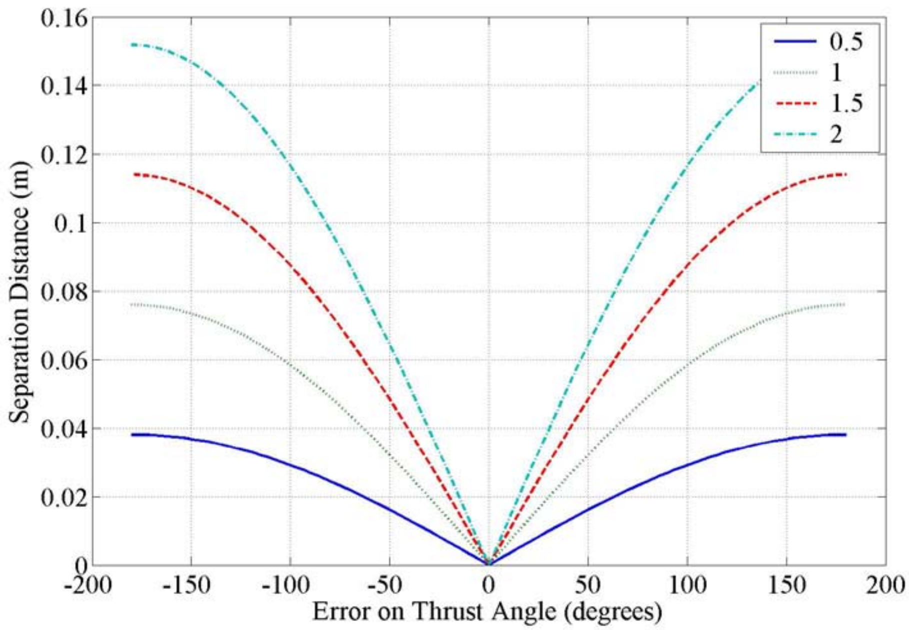

Figure 5.3: The separation distance as a function of attitude error (ψ) and initial in-track error using the f and g method.

where

$$\hat{\mathbf{T}} = \begin{bmatrix} 0 \\ -1 \\ 0 \end{bmatrix} \tag{5.38}$$

The $\mathbf{T}_{\text{ideal}}$ is expressed in the Hill coordinate frame, t_{oc} is ten seconds, and m is 100 kg. We use ten seconds as the propagation time, t, for both methods.

Exact

Figure 5.3 shows how the separation distance changes as a function of attitude error (ψ) and initial in-track error using the f and g method. When the attitude error is zero, we have the ideal case with no separation distance. As the attitude error increases the separation distance increases. We see that the separation distance is symmetric about the ideal thrust direction, but is asymmetric when larger time steps are considered. This asymmetry is caused by the orbital dynamics of the resulting orbits. When the thrust is applied with a positive attitude error, the resulting velocity vector is in a direction away from the Earth, which increases the altitude of the spacecraft. As the altitude increases the velocity of the spacecraft decreases and the period of the orbit increases. Similarly,

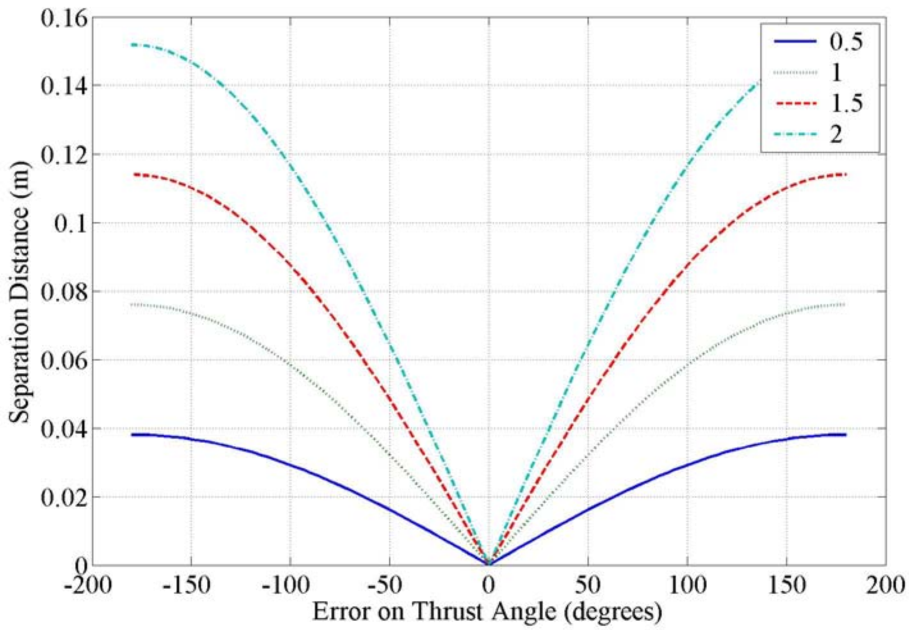

Figure 5.4: The separation distances as a function of attitude error (ψ) and initial in-track position using the Hill-Clohessy-Wiltshire equations.

when the attitude error is negative, the resultant velocity direction is towards the Earth, which causes the altitude and orbital period to decrease and the velocity to increase.

Approximate

The separation distance as a function of attitude error and initial in-track error found using the Hill-Clohessy-Wiltshire equations is shown in Figure 5.4.

Comparison

The results from the f and g method are compared to the results from the Hill-Clohessy-Wiltshire equations in Figure 5.5. This figure shows that there are differences between the results obtained using the different methods. It is difficult to see the differences between the results from each method in Figure 5.5. To examine the differences between the results we subtract the Hill-Clohessy-Wiltshire separation distances from the f and g method separation distances. These differences are shown in Figure 5.6 for all of the possible in-plane attitude errors

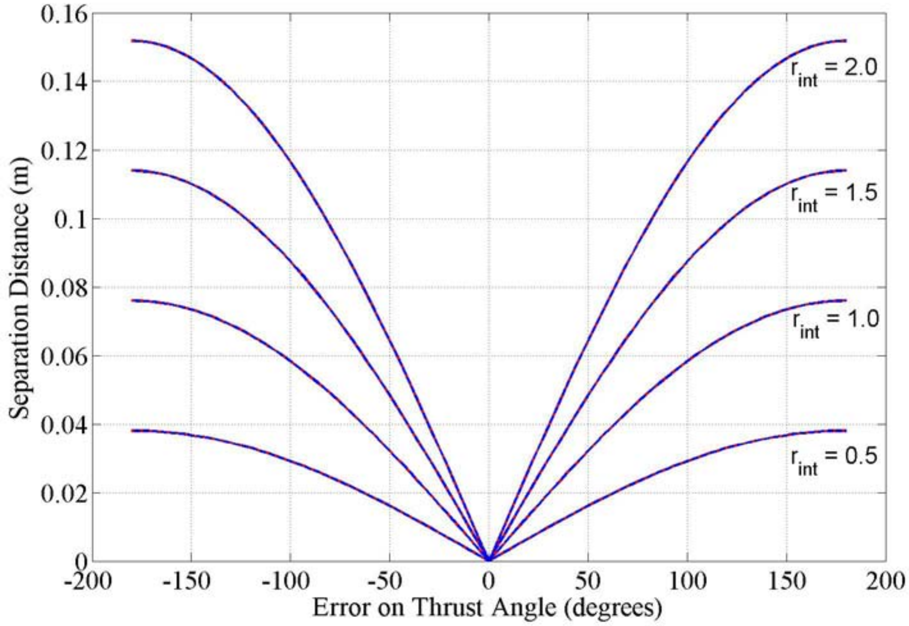

Figure 5.5: A comparison of the separation distance obtained from the two methods for all attitude errors.

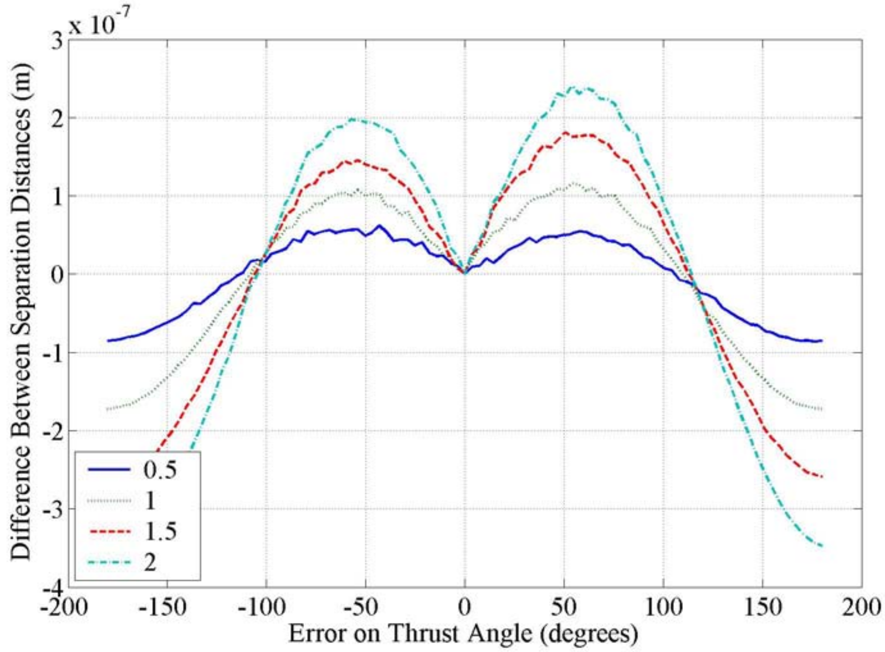

Figure 5.6: Difference between the f and g method and the Hill-Clohessy-Wiltshire equations for attitude errors of $\pm 180°$

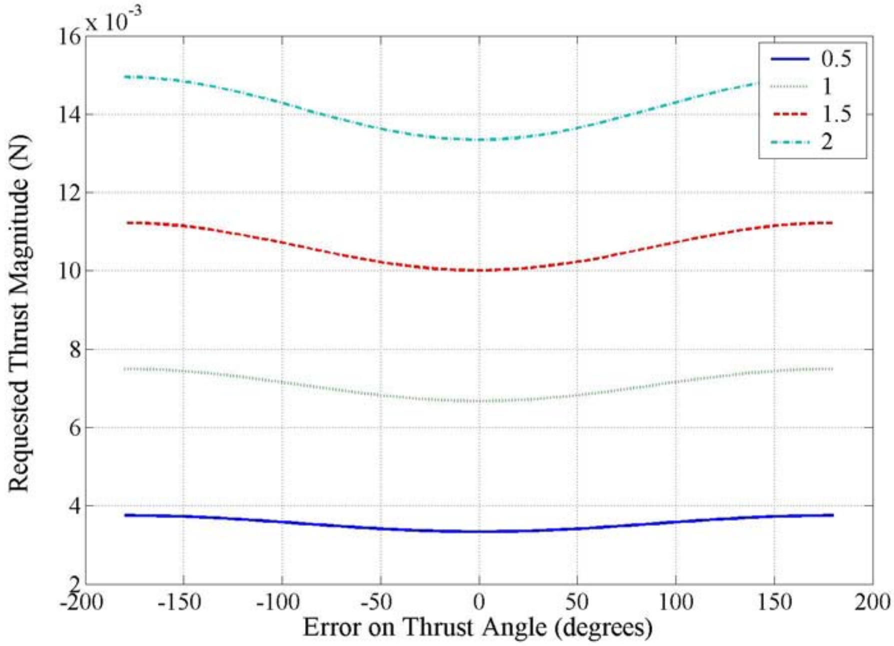

Figure 5.7: Ideal thrust magnitude at time t as a function of attitude error and initial in-track error.

These differences between the results from the two methods are small compared to the separation distances found using the two methods. The differences between the results are on the order of 10^{-7} m which is on the order of the calculation error for Matlab©. We conclude that the Hill-Clohessy-Wiltshire equations approximates the f and g method very well and can be used to determine the separation distance that would result from an attitude error.

We want to determine an allowable attitude error for the coupled system. To examine the effect of the attitude error we take the rendezvous spacecraft position at time t with an attitude error on the thrust direction ($\mathbf{r}_{t,\psi}$), and use the orbital controller to determine the magnitude of the new ideal thrust vector using the target spacecraft position ($\mathbf{t}_t$). The magnitude of this thrust vector as a function of the attitude error for the different initial in-track position errors is shown in Figure 5.7. We see that the new ideal thrust magnitude has a minimum when the attitude error is zero for each initial in-track error ($\mathbf{r}_{\text{int}}$). As the initial in-track error decreases the range of thrust magnitudes decreases. The ideal thrust magnitude at time t is a maximum when the attitude error is 180° for each initial in-track error. The ideal thrust magnitude changes by 15, 12, 13 and 11 percent for the 0.5, 1.0, 1.5, and 2.0 km initial in-track errors respectively. It is not clear how to determine the allowable attitude error from these results with a variable thrust thruster.

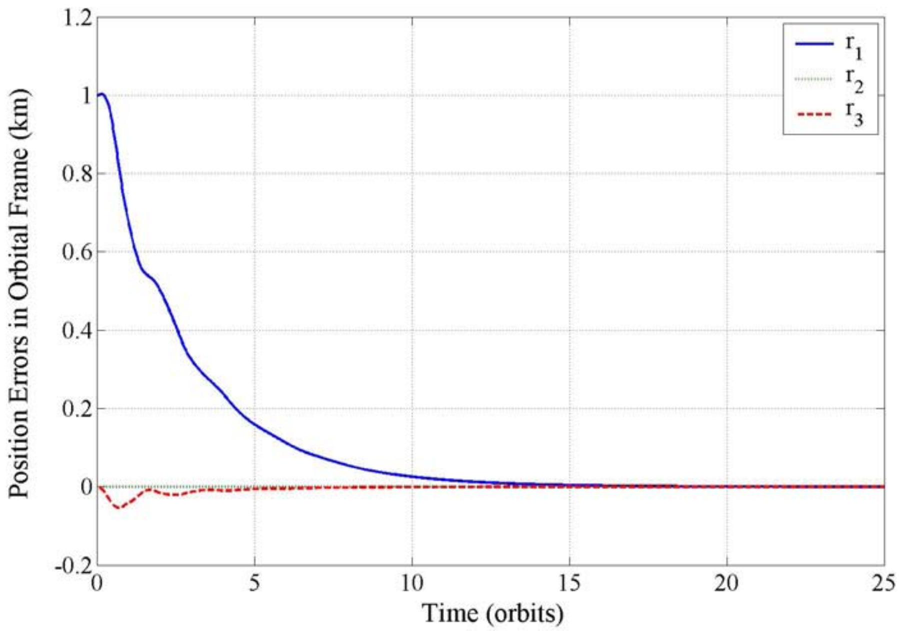

Figure 5.8: The position error in the orbital frame for a maneuver with the ideal thrust direction

We examine the effect of a constant attitude error on the total simulation time required for two spacecraft to rendezvous to determine the allowable attitude error. We define a rendezvous to be when the distance between two spacecraft is less than 10 cm and the difference between the magnitude of the velocity vector is less than 1 mm/s. We use the orbital controller with a constant attitude error on the ideal thrust direction to perform this analysis. We constrain the attitude error to be in the orbital plane which is represented by ψ in Figure 5.2.

Figure 5.8 shows how the the position error in the orbital frame varies throughout the rendezvous maneuver without an attitude error (ideal case). Figure 5.9 shows how the position error varies throughout the rendezvous maneuver with a constant attitude error of 63°. These simulations are performed using the orbital controller with an initial in-track error of 1 km. The rendezvous maneuver for the 63° attitude error case takes approximately half the time of the ideal case maneuver. We contribute this to the fact that the thrust was greater in the attitude error case. The total applied Δv is 0.06763 m/s for the ideal case and 0.18635 m/s for the 63° case. The increase in Δv for the 63° case is more than double the Δv required for the ideal case.

We present the normalized maneuver time and the required Δv to complete the rendezvous maneuver as functions of constant attitude error in Figure 5.10. The maneuver

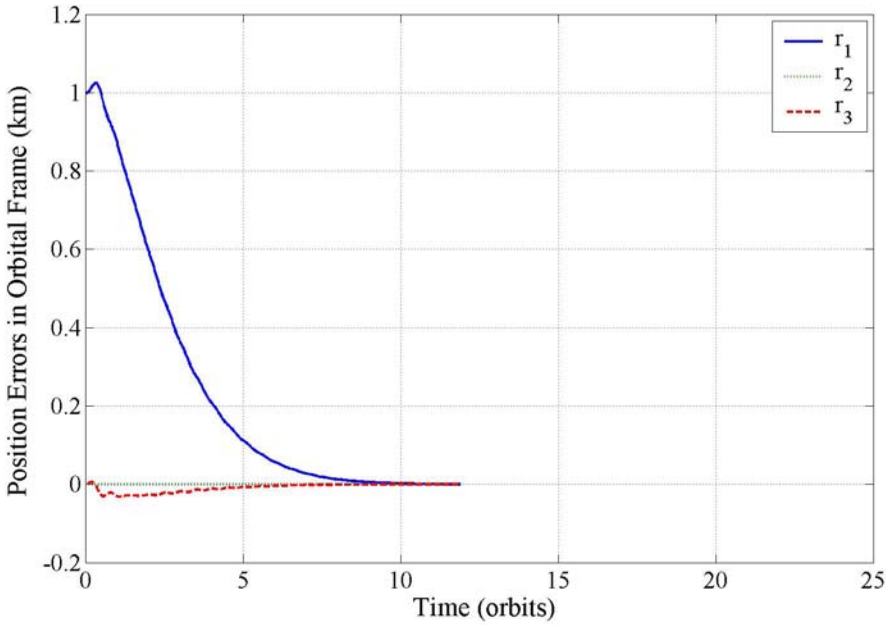

Figure 5.9: The position error in the orbital frame for a maneuver with a fixed attitude error of 63°

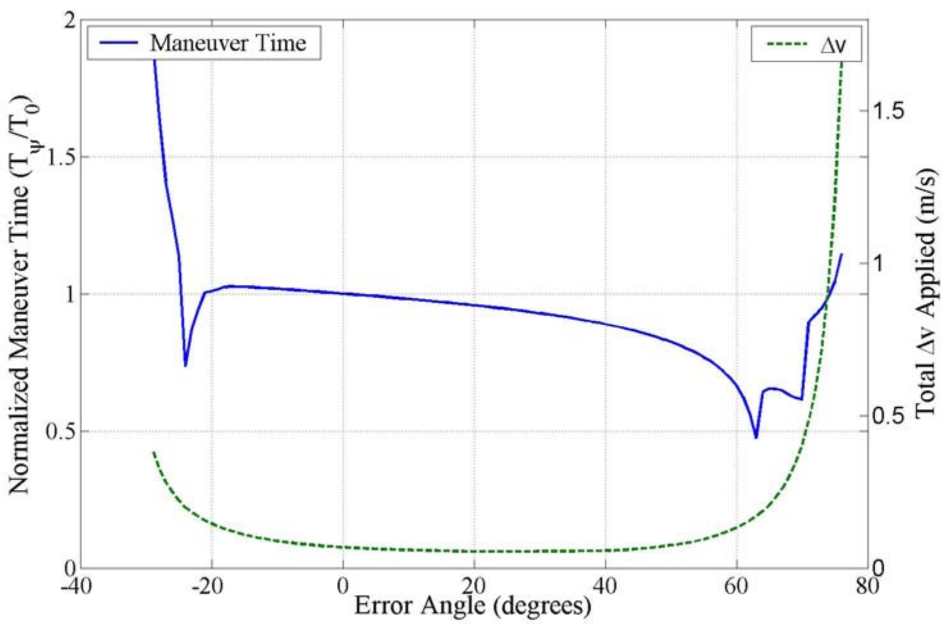

Figure 5.10: Normalized maneuver time and total required Δv as a function of attitude error

time is normalized using the maneuver time for the ideal case. We see that the ideal case without an attitude error is not the optimal case. The maneuver time decreases as the attitude error increases while requiring approximately the same amount of Δv to complete the maneuver. From this graph we determine that the allowable attitude error in the orbital plane is between -10° and 40°. This range of attitude errors is chosen because the maneuver time and required Δv are almost constant.

5.4 Summary

We have developed the overall architecture of the coupled attitude and orbital control system using a linear and nonlinear attitude controller and an orbital controller (thrust direction estimator). We have also presented the f and g method as the orbital propagator (orbital estimator) of the coupled system. We have developed a method to check the attitude of the spacecraft compared to the desired attitude of the spacecraft and examined the effect of an attitude error on the thrust direction. In the next chapter we will perform numerical simulations on the nonlinear attitude and orbital controllers and the coupled system.

Chapter 6

Numerical Simulations

We test the coupled orbital and attitude control system using simulations, but we verify the nonlinear attitude controller and the orbital controller (thrust direction estimator) separately. The simulations of the separate controllers and the coupled attitude and orbital control system are performed using Matlab©. In the following sections we discuss the attitude controller, the orbital controller and the coupled orbital and attitude control technique simulations.

6.1 Attitude Controller

We perform simulations using the nonlinear attitude controller to demonstrate that the controller is globally asymptotically stable as proven analytically in Ref. 17. The following spacecraft parameters are used

$$I = \begin{bmatrix} 6.2 & -0.9 & -0.2 \\ -0.9 & 7.5 & 0.1 \\ -0.2 & 0.1 & 12.1 \end{bmatrix} (\mathrm{kg} \cdot \mathrm{m}^2)$$

$$I_s = \begin{bmatrix} 0.075 & 0 & 0 \\ 0 & 0.075 & 0 \\ 0 & 0 & 0.075 \end{bmatrix} (\mathrm{kg} \cdot \mathrm{m}^2), \quad A = \begin{bmatrix} 1 & 0 & 0 \\ 0 & 1 & 0 \\ 0 & 0 & 1 \end{bmatrix}$$

where I is the moment of inertia matrix of the system, I_s is the moment of inertia matrix of the momentum wheels, A is the axial unit vector matrix of the momentum wheels.

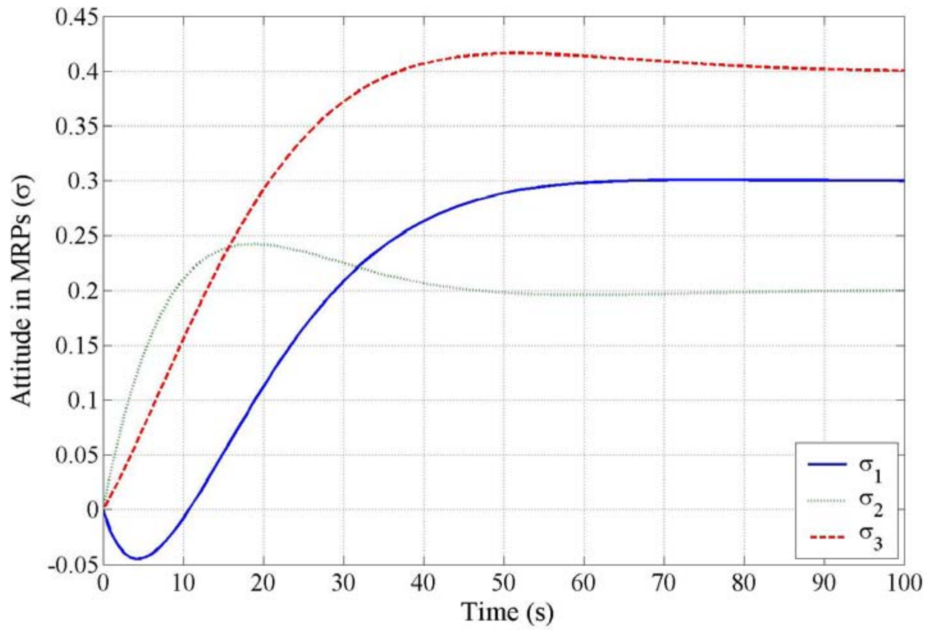

Figure 6.1: The change in the Modified Rodrigues Parameters of the spacecraft.

The following initial conditions are used

$$\boldsymbol{\omega}_i = \begin{bmatrix} -0.1 \\ 0.15 \\ 0.05 \end{bmatrix} \left(\frac{\text{rad}}{\text{s}}\right), \quad \boldsymbol{\sigma}_i = \begin{bmatrix} 0 \\ 0 \\ 0 \end{bmatrix}, \quad k_1 = 0.3, \quad k_2 = 1.5$$

$$\boldsymbol{\omega}^* = \begin{bmatrix} 0 \\ 0 \\ 0 \end{bmatrix} \left(\frac{\text{rad}}{\text{s}}\right), \quad \boldsymbol{\sigma}^* = \begin{bmatrix} 0.3 \\ 0.2 \\ 0.4 \end{bmatrix}$$

where $\boldsymbol{\omega}_i$ is the initial attitude, $\boldsymbol{\sigma}_i$ is the initial angular velocity of the system, $\boldsymbol{\sigma}^*$ is the desired attitude, $\boldsymbol{\omega}^*$ is the desired angular velocity, k_1 is the attitude gain, and k_2 is the angular velocity gain. Figure 6.1 shows how the attitude varies throughout the simulation. The attitude of the spacecraft starts at the initial conditions and proceeds to the desired attitude in approximately 80 seconds. Figure 6.2 is the variation of the body angular velocity and Figure 6.3 is the applied torque provided by the momentum wheels throughout the simulation. These figures show that the angular velocity and the applied torque start at their initial conditions and then converge to zero after approximatively 80 seconds. This simulation is representative of the attitude simulations. We conclude that the nonlinear attitude controller is effective in controlling nonlinear attitude dynamics.

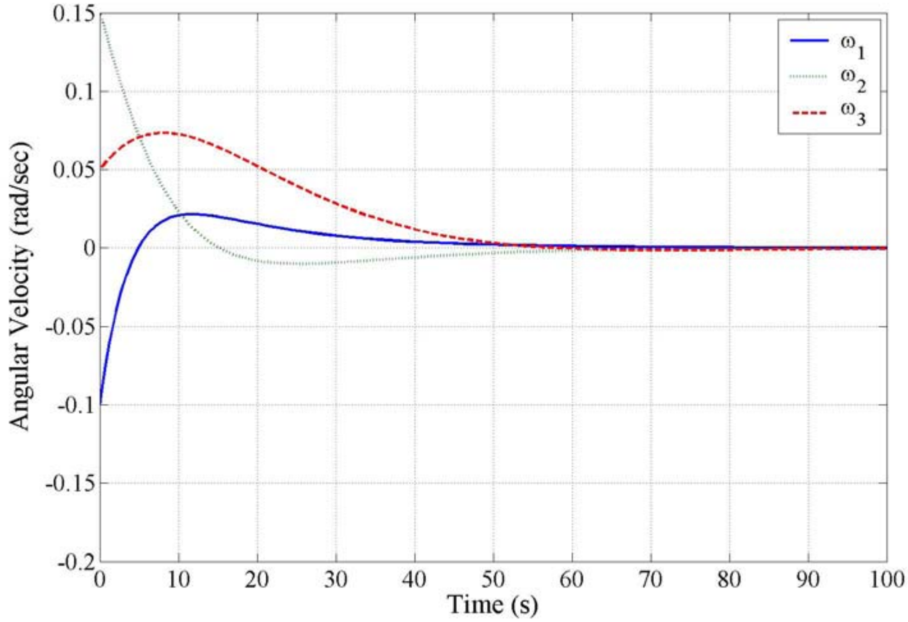

Figure 6.2: The change in the angular velocity of the spacecraft.

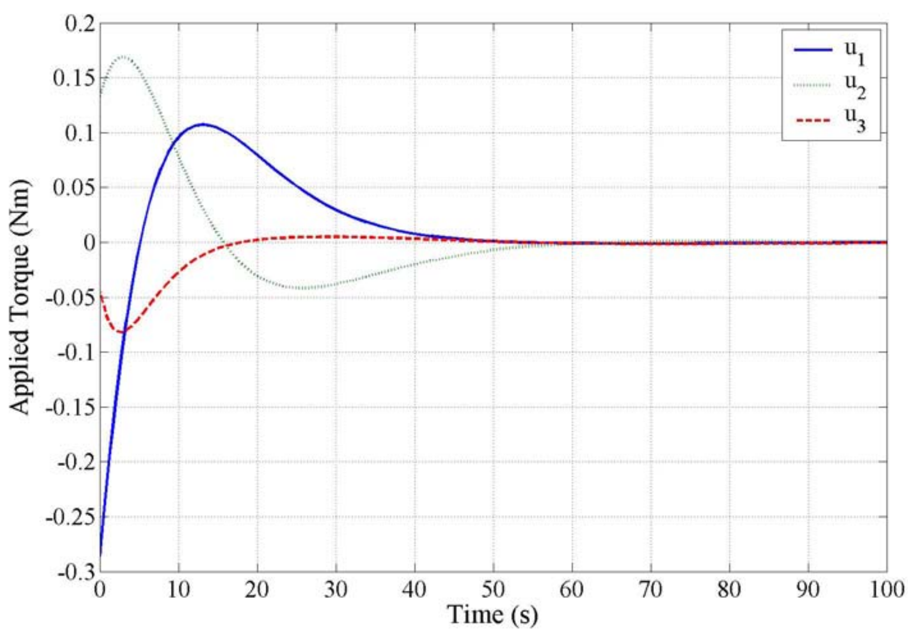

Figure 6.3: The applied torque produced by the momentum wheels.

6.2 Orbital Controller (Thrust Direction Estimator)

The orbital controller simulations are performed assuming that the spacecraft is able to apply thrust in any direction instantaneously. The initial conditions and spacecraft parameters for the simulation are

$$a^* = 6823\,(\text{km}), \quad e^* = 0.001, \quad i^* = 28^\circ, \quad \Omega^* = 135^\circ, \quad \omega^* = 90^\circ, \quad \nu = 0^\circ$$

$$\delta a = 0, \quad \delta e = 0, \quad \delta i = 0^\circ, \quad \delta\Omega = 0^\circ, \quad \delta\omega = 0^\circ, \quad \delta\nu = -\left(\frac{2}{6823}\right)^\circ$$

$$\Delta t_t = 100\,(\text{sec}), \quad m = 100\,(\text{kg}), \quad K_n = 0.05$$

where $(\cdot)^*$ are the target spacecraft orbital elements, $\delta(\cdot)$ are the change in orbital elements of the rendezvous spacecraft compared to the target spacecraft, Δt_t is the time that the thruster fires, m is the mass of the rendezvous spacecraft, and K_n is the mean motion control gain. Figure 6.4 shows the position error between the rendezvous and target spacecraft in the orbital frame. The position error between the two spacecraft becomes zero after approximately 14 orbits. Figure 6.5 shows the change in semi-major axis of the rendezvous spacecraft throughout the simulation. The semi-major axis of the rendezvous spacecraft initially starts at the same semi-major axis as the target spacecraft and then decreases as the rendezvous spacecraft lowers its orbit and then increases back to the target spacecraft semi-major axis to complete the rendezvous maneuver. Figure 6.6 is the magnitude of the thrust applied to the rendezvous spacecraft. The magnitude of the required applied thrust is on the order of millinewtons. Figure 6.7 shows the thrust direction in the orbital frame. The thrust direction changes rapidly over the course of the simulation, and switches back and forth between the positive and negative velocity direction of the rendezvous spacecraft. These figures are representative of similar simulations performed using different initial conditions. We conclude that the orbital controller is effective in formation-keeping and formation-maneuvers.

6.3 Coupled System

We have demonstrated numerically that the orbital controller (thrust direction estimator) and nonlinear attitude controller are globally asymptotically stable. We now couple these controllers according to the architecture described in Chapter 5. The coupling of the two controllers is performed so that the attitude controller can orient the spacecraft in

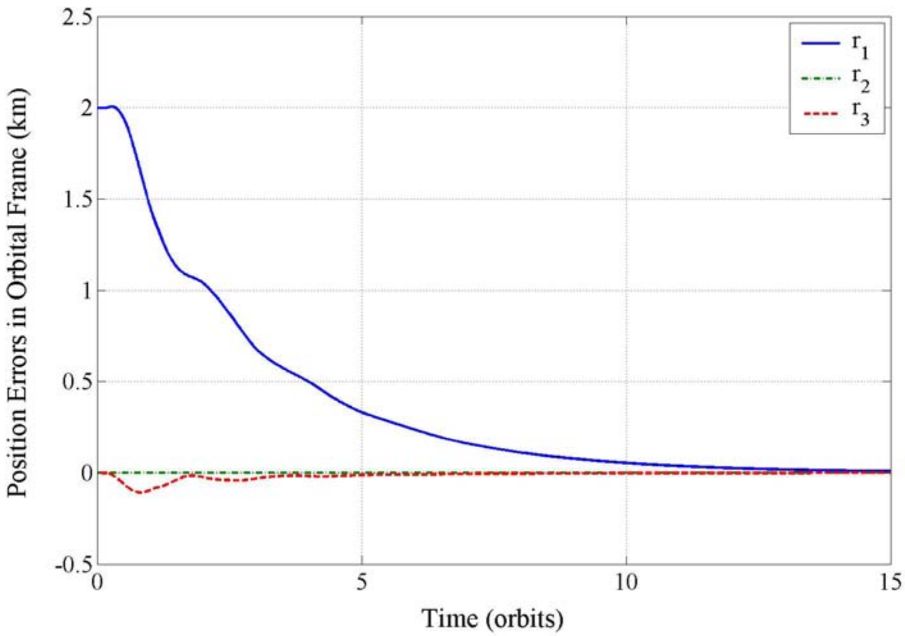

Figure 6.4: The position error in the orbital frame as seen by the rendezvous spacecraft.

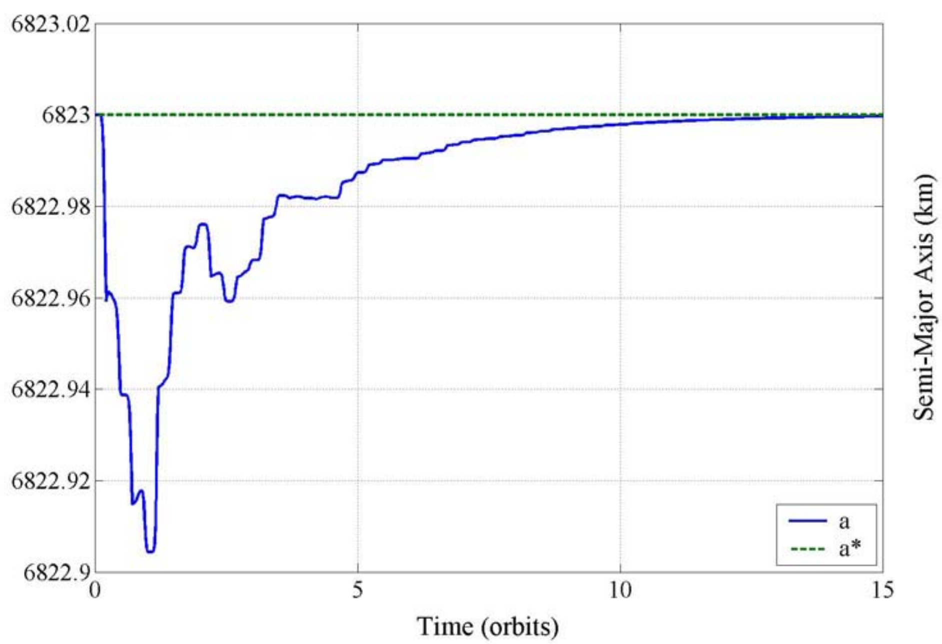

Figure 6.5: The change in semi-major axis of the rendezvous spacecraft(a) compared to the target spacecraft(a^*).

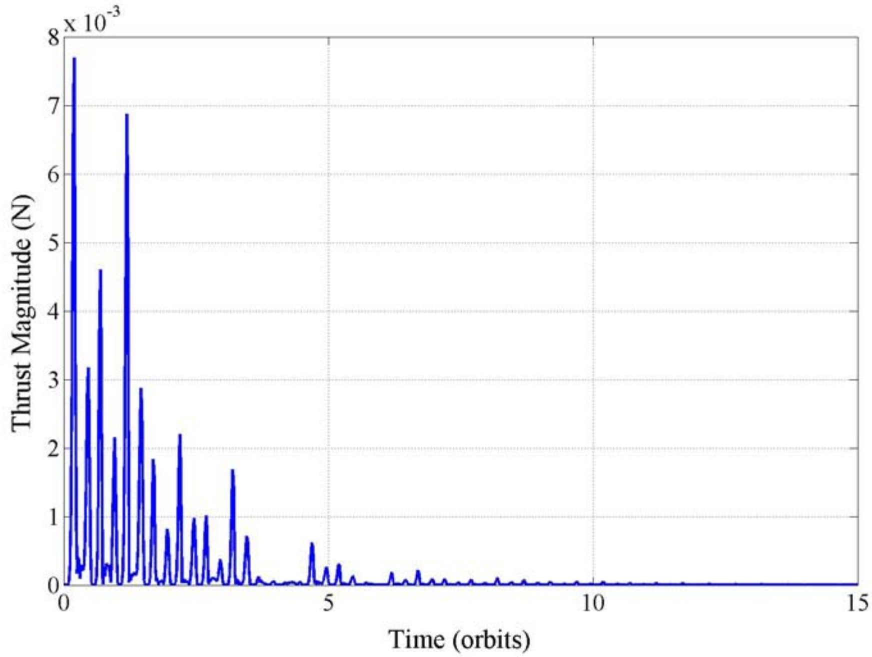

Figure 6.6: The magnitude of thrust applied to the rendezvous spacecraft.

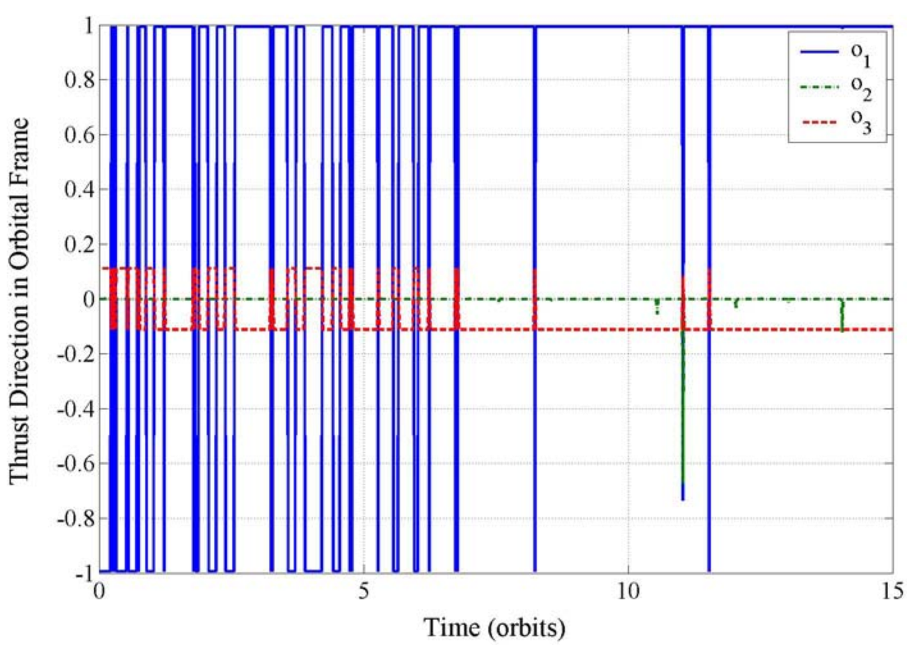

Figure 6.7: The thrust direction of the rendezvous spacecraft in the orbital frame.

the correct direction before the orbital controller can apply the thrust. The spacecraft parameters and the initial conditions for the simulation are

$$a^* = 6823\,(\text{km}), \quad e^* = 0.001, \quad i^* = 28^\circ, \quad \Omega^* = 135^\circ, \quad \omega^* = 90^\circ, \quad \nu = 0^\circ$$

$$\delta a = 0, \quad \delta e = 0, \quad \delta i = 0^\circ, \quad \delta\Omega = 0^\circ, \quad \delta\omega = 0^\circ, \quad \delta\nu = -\left(\frac{2}{6823}\right)^\circ$$

$$\Delta t_t = 100\,(\text{sec}), \quad m = 100\,(\text{kg}), \quad K_n = 0.05, \quad k_1 = 0.3, \quad k_2 = 1.5$$

$$I = \begin{bmatrix} 6.2 & -0.9 & -0.2 \\ -0.9 & 7.5 & 0.1 \\ -0.2 & 0.1 & 12.1 \end{bmatrix} (\text{kg}\cdot\text{m}^2)$$

$$I_s = \begin{bmatrix} 0.075 & 0 & 0 \\ 0 & 0.075 & 0 \\ 0 & 0 & 0.075 \end{bmatrix} (\text{kg}\cdot\text{m}^2), \quad A = \begin{bmatrix} 1 & 0 & 0 \\ 0 & 1 & 0 \\ 0 & 0 & 1 \end{bmatrix}$$

$$\boldsymbol{\omega}_i = \begin{bmatrix} 0 \\ 0 \\ 0 \end{bmatrix} \left(\frac{\text{rad}}{\text{s}}\right), \quad \boldsymbol{\sigma}_i = \begin{bmatrix} 0 \\ 0 \\ 0 \end{bmatrix}, \quad \tilde{\mathbf{T}} = \begin{bmatrix} -1 \\ 0 \\ 0 \end{bmatrix}$$

where $\tilde{\mathbf{T}}$ is the orientation of the single thruster in the body frame of the rendezvous spacecraft. Figure 6.8 shows the relative error between the rendezvous and target spacecraft in the orbital frame. The coupled controller takes approximately half an orbit longer to reach the target spacecraft than the orbital controller (Figure 6.4). This delay in the coupled system is expected and attributed to the time required to complete the attitude maneuvers. Figure 6.9 shows the variation of the semi-major axis over the simulation time. There is not much of a difference between this figure and Figure 6.5 where the semi-major axis decreases because of the mean motion control strategy and then increases as the position error decreases until the rendezvous maneuver is completed. The thrust magnitude is shown in Figure 6.10. These values are greater than the values seen in Figure 6.6. This increase in thrust magnitude is also attributed to the introduction of the time delays between the application of thrust to the spacecraft. The values for the thrust are relatively small, which is good for propulsion systems on formation flying spacecraft that require small changes in position. Figure 6.11 shows the attitude error between the desired attitude and the current attitude that was found after the attitude maneuver was completed. The allowable attitude error is also shown in Figure 6.11. The allowable attitude error is between -10° and 40° in the orbital plane and ±5° out of the orbital plane. The thruster is not fired when the attitude error is greater than

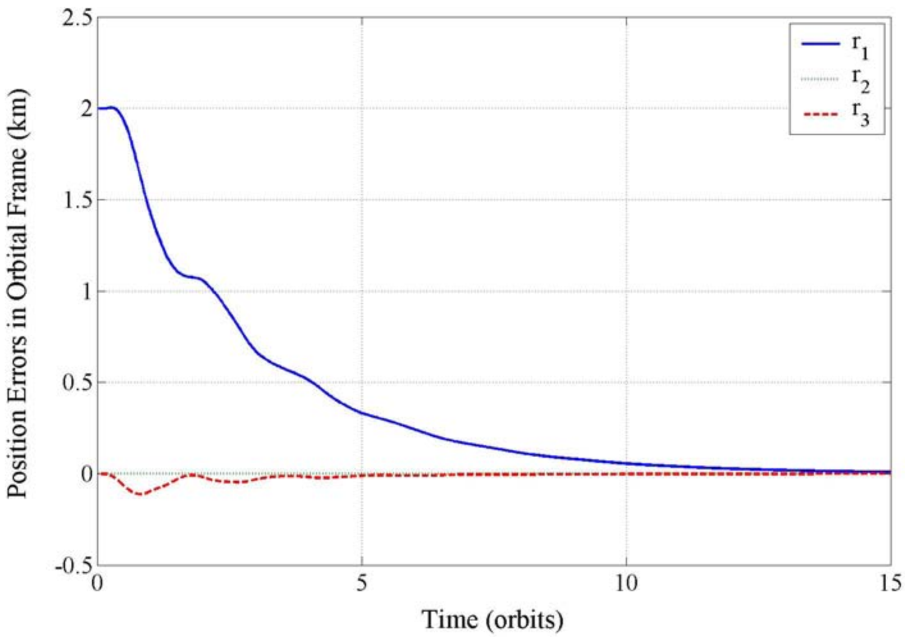

Figure 6.8: The position error in the orbital frame as seen by the rendezvous spacecraft. (coupled control)

the allowable attitude error. For this simulation the thruster fired 86% of the time. The thrust direction for the coupled system switches between the positive and negative orbit velocity direction of the rendezvous spacecraft. This variation is similar to Figure 6.7, so this graph is not included in the analysis of the coupled system. We conclude that the coupled attitude and orbital control can be used for formation flying missions while not significantly increasing the time to accomplish orbital maneuvers.

6.4 Summary

We have presented the numerical simulations for the nonlinear attitude controller, nonlinear orbital controller and the coupled attitude and orbital control system in this chapter. We have shown that the coupled system performs well when compared to the orbital controller. In the next chapter we summarize the work completed in this thesis, draw some conclusions and provide some recommendations for future work.

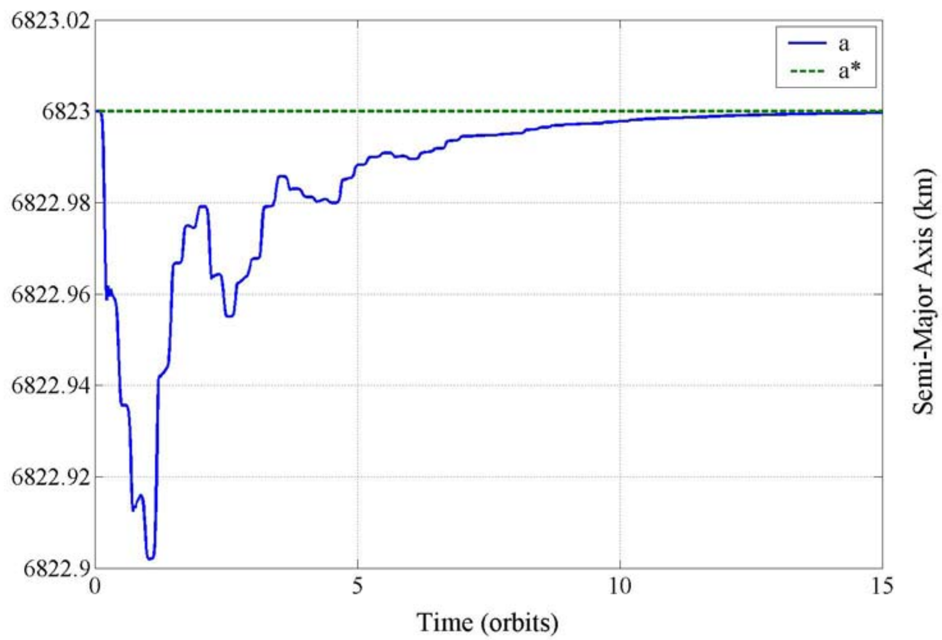

Figure 6.9: The change in semi-major axis of the rendezvous spacecraft(a) compared to the target spacecraft(a*). (coupled control)

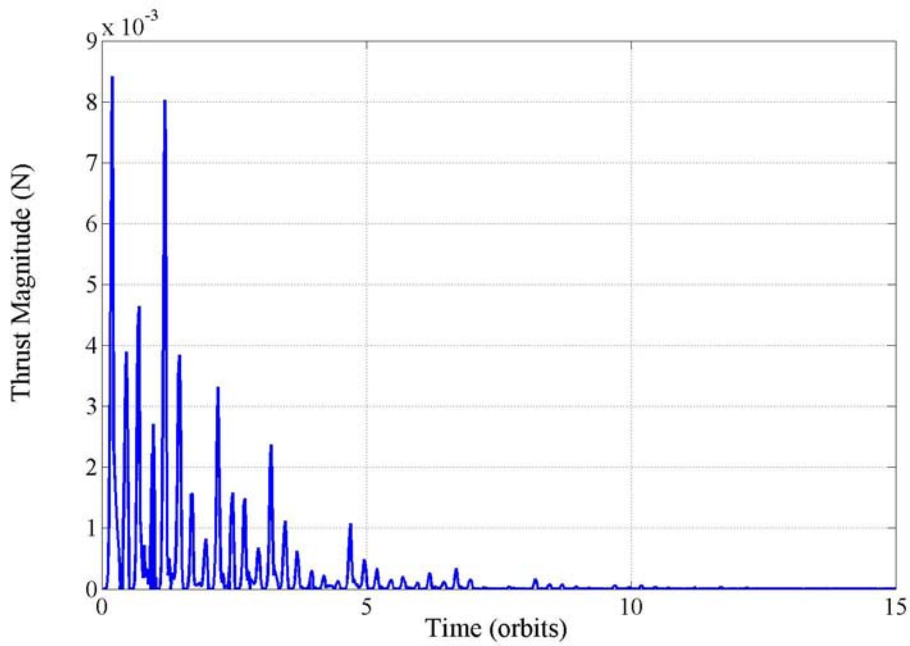

Figure 6.10: The magnitude of thrust applied to the rendezvous spacecraft. (coupled control)

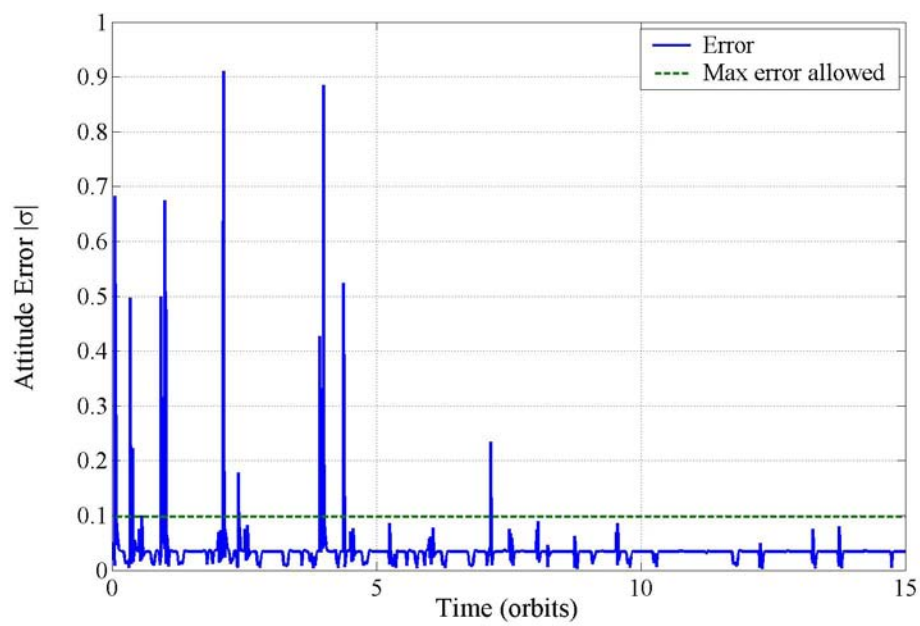

Figure 6.11: The magnitude of the error between the desired thrust direction and the actual thrust direction.

Chapter 7

Summary, Conclusions and Recommendations

In this chapter we provide a summary of the work presented in this thesis. We draw some conclusions about the coupled attitude and orbital control system and provide some recommendations for future work to be performed using the coupled system.

7.1 Summary

We have discussed the concept of coupling the attitude and orbital systems. This coupling concept is relatively new and required for spacecraft formation flying missions because the translational and rotational motion is coupled. We have presented a literature review of attitude and orbital controllers and of coupled attitude and orbital controllers.

We have presented the attitude kinematics and dynamics and the orbital dynamics associated with spacecraft formation flying missions. We presented a nonlinear Lyapunov attitude controller and a nonlinear Lyapunov-like orbital controller with mean motion control that were used in the coupled attitude and orbital control system.

We presented the coupled system architecture where a two-body orbital propagator was used to propagate the spacecraft orbit and a linear bang-bang attitude controller was used to estimate the time required by the nonlinear attitude controller to perform a given attitude maneuver. We have determined an allowable attitude error to fire the thruster. We have determined that the Hill-Clohessy-Wiltshire equations can be used to determine the effect of the attitude error for small time intervals.

We performed numerical simulations using the attitude and orbital controllers using Matlab©. We used the two attitude controllers, the orbital controller and the orbital propagator to couple the system. This coupled system was demonstrated by performing numerical simulations in Matlab©.

7.2 Conclusions

The coupled attitude and orbital control system presented in this thesis is able to correct for an initial relative position error between two spacecraft. This coupled control strategy is one of the first to use a nonlinear attitude controller and a nonlinear orbital controller for formation flying missions. The use of the nonlinear controllers allows for the nonlinear dynamics of the system to be modeled and controlled more effectively than with linear controllers. This coupled control strategy uses a linear attitude controller to estimate the time required for the nonlinear attitude controller to perform a maneuver. The time estimates provided by the linear controller where not exact, but they allowable the nonlinear controller to maneuver the attitude to within the allowable attitude error 86% of time.

The coupled system has the possibility of a negative effect on the orbital controller (thrust direction estimator). This negative effect is caused by the addition of the time required for the completion of the attitude maneuvers. The coupled control strategy presented in this thesis negatively affects the performance of the orbital controller by approximately a half an orbit. This negative affect on the orbital controller is not significant when the total orbital maneuver time is considered. The coupled control strategy increases the orbital maneuver time by 3.5%. This error is not significant because the time required to accomplish the attitude maneuvers is relatively small in comparison to the time required for the orbital maneuvers. The coupled control strategy also does not require a large propulsion system. The simulations were completed using a 100 kg spacecraft with a variable thrust propulsion system. The thrust magnitudes for the simulations were on the order of millinewtons or less.

The results found in this thesis could be improved by increasing the number of thrusters. By increasing the number of thrusters, the magnitude and thus the time required for the attitude maneuvers would be decreased. If enough thrusters were added to the spacecraft, we would reach the ideal case represented by the thrust direction estimator.

The implementation of the coupled control strategy has the ability for the substitution of different control laws with minimal changes to the overall system. This allows for the testing of many different coupled control systems which may lead to an optimal solution for a particular mission. This implementation also allows for the substitution of different orbital estimators (orbital propagators). This substitution allows for the addition of orbital perturbations and high fidelity integrators.

The coupled control strategy has been proven to work for spacecraft formation flying applications, but the implementation of coupled control strategies on single spacecraft missions could be beneficial to mission performance.

7.3 Recommendations

The coupled system presented in this thesis was developed so that it could be implemented on Virginia Tech's Distributed Spacecraft Attitude Control System Simulator (DSACSS). In the following section we discuss how the coupled system could be implemented on the DSACSS system. We also present some recommendations for future study.

7.3.1 Implementation in DSACSS

Implementing the coupled attitude and orbital control system in DSACSS requires converting the Matlab© code into the C/C++ DSACSS software architecture. The DSACSS simulators have an onboard PC/104+ form-factor computer to control the spacecraft simulators. These computers are not fast enough to control the attitude of the simulators and to run the orbital propagator and orbital controller. We require that the attitude control and attitude determination be completed onboard the spacecraft simulators and the orbital control and orbital propagation be completed on a desktop computer. A communications C++ class has been developed to allow for the PC/104+ and the desktop to communicate the required information for the coupled attitude and orbital control system.

The DSACSS system includes a Global Positioning System (GPS) Enhanced Onboard Navigation System (GEONS), which is a high fidelity orbital propagator that should be incorporated into the coupled system. The GEONS software allows for the use of a high fidelity orbital propagator and a simple two-body orbital propagator. The coupled system should be tested using the high fidelity orbital propagator after the initial testing has been completed using the two-body orbital propagator. The GEONS software is from the Goddard Space Flight Center and is discussed in Ref 51. The DSACSS system also includes a GPS simulator which is used to visually examine the relative orbits between formation flying spacecraft. In the future, it may be possible to include these GPS measurements in the coupled system to determine the effect of non-ideal orbit determination.

7.3.2 Attitude Error

It was very difficult to determine the allowable attitude error for this system, because we used a variable thrust thruster that did not have a maximum thrust. Typically, a spacecraft has a single thrust value[21] which would allow for the allowable attitude error to be determined by the limitations of the propulsion system.

Alfriend and Lovell determine that the thrust direction error is insignificant compared to the error associated with orbit determination.[52] We presented results on the separation distance on the order of millimeters. Determining the absolute position of a spacecraft within millimeters is not possible with the current technology. It is possible that formation flying spacecraft could determine their relative positions within millimeters.

Javorsek and Longuski presented the concept of changing the thrust profile for a spinning spacecraft to decrease the position error caused by the error on the thrust direction.[53] This concept might be applicable to formation flying missions and the associated attitude maneuvers required for formation keeping. More research needs to be performed to determine the effect of the attitude error has on spacecraft formation flying.

7.3.3 Controllers

This coupled control system was developed to be a modular system and to allow for other attitude and orbital controllers to be tested as a coupled system. There are numerous attitude and orbital controllers that have been developed that could be tested using this coupled system.

The linear bang-bang attitude controller can be replaced with a controller that estimates the time required for the nonlinear attitude maneuver to be completed. Schaub *et al.* presents a linear bang-bang attitude controller with a control on the sharpness of the applied torque switches that could increase the accuracy of the time estimate function.[54]

This coupled system was developed assuming that the propulsion system had a variable thrust thruster and that the thrust was always applied at the center of mass of the spacecraft. This concept needs to be expanded to include a more realistic propulsion system and propulsion systems that induce torques on the attitude of the spacecraft.

References

[1] K. Lasswitz, *Two planets: Auf zwei Planeten*. Carbondale, Southern Illinois University Press, 1971. Orginially published in 1897 by Leipzig in Germany.

[2] T. Mel'kumov, ed., *Pioneers of Rocket Technology: Selected Works*, ch. Review by Mechanical Engineer V. P. Vetchinkin of Yu. Kondratyuk's Article 'On Interplanetary Voyages', p. 114. Moscow, 1964. NASA TT F-9285 – 1965, Article orginially published in 1916 in the Ukraine.

[3] E. C. Ezell and L. N. Ezell, *The Partnership: A History of the Apollo-Soyuz Test Project*. The NASA History Series, NASA SP-4290, 1978. Available at www.apolloexplorer.co.uk/books/sp-4209/cover.htm.

[4] "Submillimeter Probe of the Evolution of Cosmic Structure." http://space.gsfc.nasa.gov/astro/specs/, Last accessed June 4, 2004.

[5] "Terrestrial Planet Finder." http://planetquest.jpl.nasa.gov/TPF/tpf_index.html, Last accessed June 4, 2004.

[6] "Space Technology 5: Tomorrow's Technology Today." http://nmp.jpl.nasa.gov/st5/, Last accessed June 4, 2004.

[7] J. A. Leitner, "Formation Flying," in *Proceedings of the Technology Planning Workshop for Space Technology 9 (ST9)*, (Washington, D.C.), February 5–6, 2003.

[8] "Aura: Atmospheric Chemistry." http://aura.gsfc.nasa.gov/mission/index.html, Last accessed June 4, 2004.

[9] J. L. Schwartz and C. D. Hall, "The Distributed Spacecraft Attitude Control System Simulator: Development, Progress, Plans," NASA Space Flight Mechanics Symposium, Greenbelt, Maryland, February 27-31, 2003.

[10] "Geospace Electrodynamic Connections." http://stp.gsfc.nasa.gov/missions/gec/gec.htm, Last accessed June 22, 2004.

[11] "HokieSat: Virginia Tech's First Satellite." http://www.aoe.vt.edu/ hokiesat/, Last accessed June 22, 2004.

[12] "LISA: Laser Interferometer Space Antenna Project Office." http://lisa.gsfc.nasa.gov/, Last accessed June 22, 2004.

[13] "Magnetospheric Multiscale." http://mms.gsfc.nasa.gov/, Last accessed June 22, 2004.

[14] "TechSat21 Next Generation Space Capabilities." http://www.vs.afrl.af.mil/TechProgs/TechSat21/NGSC.html, Last accessed June 22, 2004.

[15] J. R. Wertz and W. J. Larson, eds., *Space Mission Analysis and Design.* Space Technology Series, Microcosm Press, Torrance, California and Kluwer Academic Publishers, Dirdrecht / Boston / London, third ed., 1999.

[16] P. Tsiotras, "New Control Laws for the Attitude Stabilization of Rigid Bodies," pp. 316–321, 13th IFAC Symposium on Automatic Control in Aerospace, Palo Alto, California, September 12–16, 1994.

[17] C. D. Hall, P. Tsiotras, and H. Shen, "Tracking Rigid Body Motion Using Thrusters and Momentum Wheels," *The Journal of the Astronautical Sciences*, vol. 50, no. 3, pp. 311–323, 2002.

[18] P. Tsiotras, H. Shen, and C. D. Hall, "Satellite Attitude Control and Power Tracking with Energy/Momentum Wheels," *Journal of Guidance, Control and Dynamics*, vol. 24, pp. 23–34, January–February 2001.

[19] H. Schaub, M. R. Akella, and J. L. Junkins, "Adaptive Control of Nonlinear Attitude Motions Realizing Linear Closed Loop Dynamics," *Journal of Guidance, Control and Dynamics*, vol. 24, pp. 95–100, January–February 2001.

[20] G. Q. Xing and S. A. Parvez, "Nonlinear Attitude State Tracking Control for Spacecraft," *Journal of Guidance, Control and Dynamics*, vol. 24, pp. 624–626, May–June 2001.

[21] R. W. Humble, G. N. Henry, and W. J. Larson, eds., *Space Propulsion Analysis and Design.* Space Technology Series, McGraw-Hill Companies, Inc., New York, New York, 1995.

[22] G. W. Hill, "Researches in the Lunar Theory," *American Journal of Mathematics*, vol. 1, no. 1, pp. 5–26, 1878.

[23] W. Clohessy and R. Wiltshire, “Terminal Guidance System for Satellite Rendezvous,” *Journal of the Aerospace Sciences*, vol. 27, pp. 653–674, September 1960.

[24] V. Kapila, A. G. Sparks, J. M. Buffington, and Q. Yan, “Spacecraft Formation Flying: Dynamics and Control,” *Journal of Guidance, Control and Dynamics*, vol. 23, pp. 561–564, May–June 2000.

[25] C. Sabol, R. Burns, and C. A. McLaughlin, “Satellite Formation Flying Design and Evolution,” *Journal of Spacecraft and Rockets*, vol. 38, pp. 270–278, March–April 2001.

[26] R. H. Vassar and R. B. Sherwood, “Formation Keeping for a Pair of Satellites in a Circular Orbit,” *Journal of Guidance, Navigation and Control*, vol. 8, pp. 235–242, March–April 1985.

[27] S. Vaddi and S. R. Vadali, “Linear and Nonlinear Control Laws for Formation Flying,” AAS/AIAA Space Flight Mechanics Meeting, Ponce, Puerto Rico, February 9–13, 2003. AAS 03-109.

[28] H. Schaub and K. T. Alfriend, “Hybrid Cartesian and Orbit Element Feedback Law for Formation Flying Spacecraft,” *Journal of Guidance, Control and Dynamics*, vol. 25, pp. 387–393, March–April 2002.

[29] H. Schaub, S. R. Vadali, J. L. Junkins, and K. T. Alfriend, “Spacecraft Formation Flying Control using Mean Orbit Elements,” *Journal of the Astronautical Sciences*, vol. 48, pp. 69–87, January–March 2000.

[30] M. R. Ilgen, “Low Thrust OTV Guidance Using Lyapunov Optimal Feedback Control Techniques,” *Advances in the Astronautical Sciences*, vol. 85, no. Part 2, pp. 1527–1545, 1993.

[31] B. J. Naasz, “Classical Element Feedback Control for Spacecraft Orbital Maneuvers,” Master’s thesis, Virginia Polytechnic Institute and State University, Blacksburg, Virginia, May 2002.

[32] P. Wang and F. Hadaegh, “Coordination and Control of Multiple Microspacecraft Moving in Formation,” *The Journal of the Astronautical Sciences*, vol. 44, pp. 315–355, July–September 1996.

[33] D. Fragopoulos and M. Innocenti, “Autonomous Spacecraft 6DOF Relative Motion Control using Quaternions and H-infinity Methods,” AIAA Guidance, Navigation and Control Conference, San Diego, California, July 29-31, 1996. AIAA-96-3725.

[34] N. Philip and M. Ananthasayanam, "Relative Position and Attitude Estimation and Control Schemes for the Final Phase of an Autonomous Docking Mission of Spacecraft," *Acta Astronautica*, vol. 52, pp. 511–522, 2003.

[35] J. M. Kruep, "Six Degree of Freedom Optimal Trajectories for Satellite Rendezvous," Master's thesis, Virginia Polytechnic Institute and State University, Blacksburg, Virginia, May 1996.

[36] H. Pan and V. Kapila, "Adaptive Nonlinear Control for Spacecraft Formation Flying with Coupled Translational and Attitude Dynamics," 40th IEEE Conference on Decision and Control, Orlando, Florida, December, 2001. IEEE-0-7803-7061-9/01.

[37] K. Yamanaka, "Simultaneous Translation and Rotation Control Law for Formation Flying Satellites," AIAA Guidance, Navigation and Control Conference and Exhibit, Denver, Colorado, August 14–17, 2000. AIAA-2000-4440.

[38] D. D. Redding, B. A. Persson, and E. V. Bergmann, "Combined Solution of Spacecraft Rotational and Translational Manuevers," AIAA Guidance, Navigation and Control Conference, Williamsburg, Virginia, August 18–20, 1986. AIAA-86-2106.

[39] B. J. Naasz, M. M. Berry, H. Y. Kim, and C. D. Hall, "Integrated Orbit and Attitude Control for a Nanosatellite with Power Constraints," AAS/AIAA Space Flight Mechanics Conference, Ponce, Puerto Rico, February 9-12, 2003. AAS 03-100.

[40] K. L. Makovec, "A Nonlinear Magnetic Controller for Nanosatellite Applications," Master's thesis, Virginia Polytechnic Institute and State University, Blacksburg, Virginia, May 2001.

[41] K. L. Makovec, A. J. Turner, and C. D. Hall, "Design and Implementation of a Nanosatellite Attitude Determination and Control System," in *Proceedings of the 2001 AAS/AIAA Astrodynamics Specialists Conference*, Quebec City, Quebec, 2001.

[42] J. L. Schwartz, M. A. Peck, and C. D. Hall, "Historical Review of Spacecraft Simulators," *Journal of Guidance, Control and Dynamics*, vol. 26, pp. 513–522, July–August 2003.

[43] H. Schaub and J. L. Junkins, *Analytical Mechanics of Space Systems.* American Institute of Aeronautics and Astronautics, Reston, Virginia, 2003.

[44] M. D. Shuster, "A Survey of Attitude Representations," *The Journal of the Astronautical Sciences*, vol. 41, no. 4, pp. 439–517, 1993.

[45] H. Schaub and J. L. Junkins, "Stereographic Orientation Parameters for Attitude Dynamics: A Generalization of the Rodrigues Parameters," *The Journal of the Astronautical Sciences*, vol. 44, pp. 1–19, January–March 1996.

[46] C. D. Hall, "AOE 4140 Spacecraft Dynamics and Control Lecture Notes." Available at www.aoe.vt.edu/˜cdhall/courses/aoe4140/, 2003.

[47] R. R. Bate, D. D. Mueller, and J. E. White, *Fundamentals of Astrodynamics.* Dover Publications, New York, New York, 1971.

[48] R. H. Battin, *An Introduction to the Mathematics and Methods of Astrodynamics, Revised Edition.* American Institute of Aeronautics and Astronautics, Reston, Virginia, 1999.

[49] K. Ogata, *System Dynamics.* Printice Hall, Upper Saddle River, New Jersey, third ed., 1998.

[50] H. K. Khalil, *Nonlinear Systems.* Macmillan Publishing Company, New York, New York, 1992.

[51] J. R. Carpenter, *Global Positioning System (GPS) Enhanced Onboard Navigation System, System Description and User's Guide.* Goddard Space Flight Center, Greenbelt, Maryland, December 2003. Version 2, Release 2.1.

[52] K. T. Alfriend and T. A. Lovell, "Error Analysis of Satellite Formations in Near-Circular Low-Earth Orbits," AAS/AIAA Astrodynamics Specialists Conference, Big Sky, Montana, August 3–7, 2003. AAS 03-651.

[53] D. Jacorsek II and J. M. Longuski, "Effect of Thrust Profile on Velocity Pointing Errors of Spinning Spacecraft," AAS/AIAA Astrodynamics Specialists Conference, Big Sky, Montana, August 3–7, 2003. AAS 03-516.

[54] H. Schaub, R. D. Robinett, and J. L. Junkins, "Globally Stable Feedback Laws for Near-Minimum-Fuel and Near-Minimum-Time Pointing Maneuvers for a Landmark-Tracking Spacecraft," *The Journal of the Astronautical Sciences*, vol. 44, pp. 443–466, October–December 1996.

Vita

Scott Evan Lennox was born on July 27, 1980 in Buffalo, New York. Scott moved to Charlottesville, Virginia in 1984 with his mother, Linda Blum, and his step-father, Aaron Mills. He attended the Charlottesville City Schools while spending the summers in North Tonawanda, New York with his father, David Lennox, and his step-mother, Rebecca Lennox. Scott graduated from Charlottesville High School in 1998. He attended Virginia Tech where he studied Aerospace Engineering in the Aerospace and Ocean Engineering Department. Scott earned his Bachelor of Science Degree in May 2002, and defended his Master of Science Degree in Aerospace Engineering on July 7, 2004.

While at Virginia Tech, Scott was involved in many extracurricular activities including Virginia Tech's Marching Band (The Marching Virginians), the American Institute of Aeronautics and Astronautics, Students for the Exploration and Development of Space, and the Aerospace Honor Society, Sigma Gamma Tau. Some of the projects Scott was involved with were the Virginia Tech Zero-G Team, the Virginia Tech Ionospheric Scintillation Measurement Mission (a.k.a HokieSat), the Virginia Satellite for Carbon-monoxide Analysis and Tabulation (a.k.a. VASCAT and MicroMAPS), and the Distributed Spacecraft Attitude Control System Simulator (DSACCS) in the Space Systems Simulation Laboratory.